ELSEVIER

Journal of Structural Geology xx (0000) xxx–xxx

JOURNAL OF STRUCTURAL GEOLOGY

www.elsevier.com/locate/jsg

Processes controlling vertical coupling and decoupling between the upper and lower crust of orogens: results from Fiordland, New Zealand

Keith A. Klepeis[a,*], Geoffrey L. Clarke[b], George Gehrels[c], Jeff Vervoort[c]

[a]*Department of Geology, University of Vermont, Burlington, VT, 05405-0122, USA*
[b]*School of Geosciences, Division of Geology and Geophysics, University of Sydney, NSW 2006, Australia*
[c]*Department of Geosciences, University of Arizona, Tucson, AZ 85721, USA*

Received 27 January 2002; received in revised form 15 July 2003; accepted 25 August 2003

Abstract

The pre-Cenozoic configuration of western New Zealand allows determination of the effects of magmatism and a changing lower crustal rheology on the evolution of a Cretaceous orogen from upper to lower crustal levels (10–50 km). Beginning at ~126 Ma, a composite batholith dominated by diorite was emplaced into the lower crust. During emplacement, deformation was partitioned into zones weakened by magma and heat, leading to the development of two layer-parallel shear zones at the upper and lower contacts of the batholith. Transient vertical decoupling of the crust above and below the batholith occurred from ~126 Ma until ~120 Ma as magma was emplaced into and moved through a weak, thick lower crust. By ~116 Ma, however, much of the batholith had crystallized and the lowermost crust had cooled from 750 °C < T < 850 °C to T = 650–700 °C. Cooling was aided by the juxtaposition of pre-existing crust against hot new crust and by the efficient extraction of partial melts out of the lower crust. Cooling together with dehydration of the lower crust and mafic compositions led to the development of a strong, dry, lower crustal root by ~116 Ma. A strong lower crust resulted in high degrees of vertical coupling between the upper and lower crust during contraction from ~116 to ~105 Ma even as magma continued to be emplaced into the mid-upper crust. A narrow, focused orogenic style in the upper crust at this time reflected a highly viscous lower crust through which compressional stresses were transferred vertically. The results imply that changes in plate boundary dynamics rather than the thermal weakening of thick lower crust during convergence controlled the onset of regional extension at ~108–105 Ma.

Keywords: Vertical coupling and decoupling; Magmatism; Orogen

1. Introduction

Studies of convergent margins worldwide have shown that deformation patterns and the mechanical behavior of continental crust vary according to crustal level and tectonic setting (e.g. Sisson and Pavlis, 1993; Axen et al., 1998; Klepeis and Crawford, 1999; Miller and Paterson, 2001; Karlstrom and Williams, 2002; Teyssier et al., 2002). Experimental data (Wilks and Carter, 1990; Rushmer, 1995; Rutter and Neumann, 1995), numerical simulations (Harry et al., 1995; Ellis et al., 1998; McKenzie et al., 2000), and analytical models (Royden, 1996) indicate that lower crustal strength and rheology especially affect how deformation is partitioned vertically through the lithosphere during convergence. These studies emphasize the critical role the lower crust plays in linking the upper mantle with the upper crust of orogens.

Despite this work, however, we still lack direct information on the mechanisms by which deformation is relayed vertically between different sections of the lithosphere, especially as physical and chemical conditions in the lower crust change. Large, dipping shear zones that divide the crust and upper mantle into different structural domains have been observed or postulated in many orogenic belts (Oldow et al., 1990; Harry et al., 1995; Willett, 1998; McKenzie et al., 2000; Teyssier et al., 2002) but we do not fully understand how deformation above, below, and within these potentially transient features relate to one another or affect orogenic evolution. This gap in knowledge arises partly because orogens that allow direct observation of processes at lower crustal levels and their relationship with the upper crust are rare. In addition, the age and kinematic

* Corresponding author. Tel.: +1-802-656-0246; fax: +1-802-656-0045.
E-mail address: keith.klepeis@uvm.edu (K.A. Klepeis).

0191-8141/$ - see front matter © 2003 Published by Elsevier Ltd.
doi:10.1016/j.jsg.2003.08.012

significance of lower crustal fabrics identified in geophysical studies (e.g. Warner, 1990; Mayer et al., 1997; Nemes et al., 1997) commonly are difficult to confirm.

In this paper, we show how displacements were transferred vertically from lower to upper crustal levels of an ancient orogen by reconstructing pieces of a composite crustal column now exposed in Fiordland and Westland (Fig. 1). This approach is possible because of the exposure of an Early Cretaceous mid–lower crustal section in Fiordland (Fig. 1; 25–50 km paleodepths) and its originally contiguous mid–upper crust in Westland (Fig. 1; 8–27 km paleodepths). The Alpine Fault now separates rocks of the Fiordland belt from those of similar Early Cretaceous and older affinity in Westland. Excellent pre-Cenozoic markers, including the western margin of the Median Batholith (Fig. 1, inset), indicate that ~460 km of offset have accumulated along the Alpine Fault (Wellman, 1953; Molnar et al., 1999; Sutherland et al., 2000). Once restored to their pre-Cenozoic configuration, the Fiordland and Westland regions form parts of the same orogenic belt (Fig. 1; Oliver, 1990; Tulloch and Challis, 2000). Mid–late Cretaceous extension exhumed much of the lower crustal parts of the belt in Fiordland as parts of the upper plate (including Westland) slid off to the SW and NE (Gibson et al., 1988; Tulloch and Kimbrough, 1989; Gibson, 1990; Oliver, 1990). By ~90 Ma, the Fiordland rocks had cooled to <400 °C and were in the upper 10 km of the crust (Mattinson et al., 1986; Nathan et al., 2000; Claypool et al., 2002). The results of this differential exhumation and offset allowed us to compare processes and events from ~126–90 Ma in Fiordland with those that occurred during the same time interval at upper crustal levels in Westland.

We present structural, metamorphic and geochronologic data that reveal the evolution of shear zones that separate the middle and lower crustal section into distinctive structural domains. We compare these features to structural patterns and events preserved in the mid–upper crust and describe how strain was partitioned within the orogen during a transition from lithospheric contraction to extension. The data indicate that strong physical and kinematic links were established between the different layers of the lithosphere only a few (~3–4 Ma) million years after emplacement of a major batholith in the lower crust. The results provide direct physical evidence of transient vertical decoupling followed by coupling between the upper and lower crust during the period ~126–105 Ma. We discuss the controls on coupling and decoupling processes and explain why the mechanical behavior of the Fiordland–Westland orogen may differ from other orogens that experienced larger degrees of partial melting and pluton emplacement in the deep crust.

2. The Fiordland–Westland orogen

The Fiordland–Westland orogen (Fig. 1) records a history of magmatism, metamorphism and deformation that accompanied the development of an early Mesozoic arc along the margin of Gondwana. A Western Belt (Fig. 1), representing the ancient continental margin, contains Paleozoic terranes that preserve a record of mostly ~380–300 Ma pluton emplacement, low- to high-grade metamorphism, and convergence (Landis and Coombs, 1967; Bishop et al., 1985; Cooper and Tulloch, 1992; Muir et al., 1996; Ireland and Gibson, 1998). An Eastern Belt (Fig. 1) contains plutons and volcano-sedimentary terranes that originally formed outboard of the margin during the early Mesozoic (Mattinson et al., 1986; McCulloch et al., 1987; Tulloch and Kimbrough, 2003). Between these two provinces (Fig. 1) is a linear, N- and NE-trending belt of early Mesozoic plutonic, volcanic and sedimentary rock called the Median Tectonic Zone (Kimbrough et al., 1994; Muir et al., 1994) or the Median Batholith (Mortimer, 1999a,b).

The Median Batholith contains several compositionally distinctive plutonic suites. On the outboard (east) side of the Gondwana margin, the Median Suite of Mortimer and Tulloch (1996) and the Darran Suite (Fig. 2) of Muir et al. (1998) were emplaced into a Permo–Triassic accretionary complex (Brook Street terrane, Fig. 1) mostly during the interval 170–128 Ma (Mortimer, 1999). These suites are dominated by diorite although gabbro and smaller granite plutons also are common. On the continent side of the Median Batholith is a younger belt of ~126–105 Ma plutonic rock that includes the Separation Point and Rahu suites (Fig. 1; Bradshaw, 1990; Kimbrough et al., 1994; Muir et al., 1994; Mortimer et al., 1999a; Tulloch and Kimbrough, 2003). At mid–upper crustal levels, now exposed in Westland and easternmost Fiordland, rocks of these latter two suites are dominated by tonalitic, granodioritic and granitic compositions. The lower crustal levels of this belt, exposed in Fiordland, are represented by the dioritic–monzodioritic Western Fiordland Orthogneiss (WFO; Figs. 1 and 2). Gabbro also is common in the WFO.

The emplacement of plutons of the Separation Point Suite into both Eastern and Western belts at ~126 Ma indicate that these two provinces were together at that time

Fig. 1. Present configuration (top of inset) and Cretaceous reconstruction (bottom of inset and main diagram) of western New Zealand after Tulloch and Challis (2000). Geologic relationships are from Wood (1972), Oliver and Coggon (1979), Bradshaw (1989), Daczko et al. (2002a) and Klepeis and Clarke (2003). Abbreviations show key locations or features: MB—Median Batholith, SP—Separation Point, L—Largs Terrane; MS—Milford Sound; GS—George Sound; CS—Caswell Sound; CHS—Charles Sound; DS—Doubtful Sound; LTA—Lake Te Anau; LM—Lake Manapouri. Metamorphic pressures from Fiordland represent the peak of Early Cretaceous metamorphism at ~120 Ma and are from Bradshaw (1985, 1989a,b), Brown (1996), Klepeis et al. (1999), Clarke et al. (2000) and Daczko et al. (2001a,b, 2002a,b). See text for discussion. Pressures from Westland show shallower early–mid-Cretaceous (125–105 Ma) pluton emplacement depths (after Tulloch and Challis, 2000). Metamorphic and structural data from Fiordland show a south-tilted lower crustal section (b).

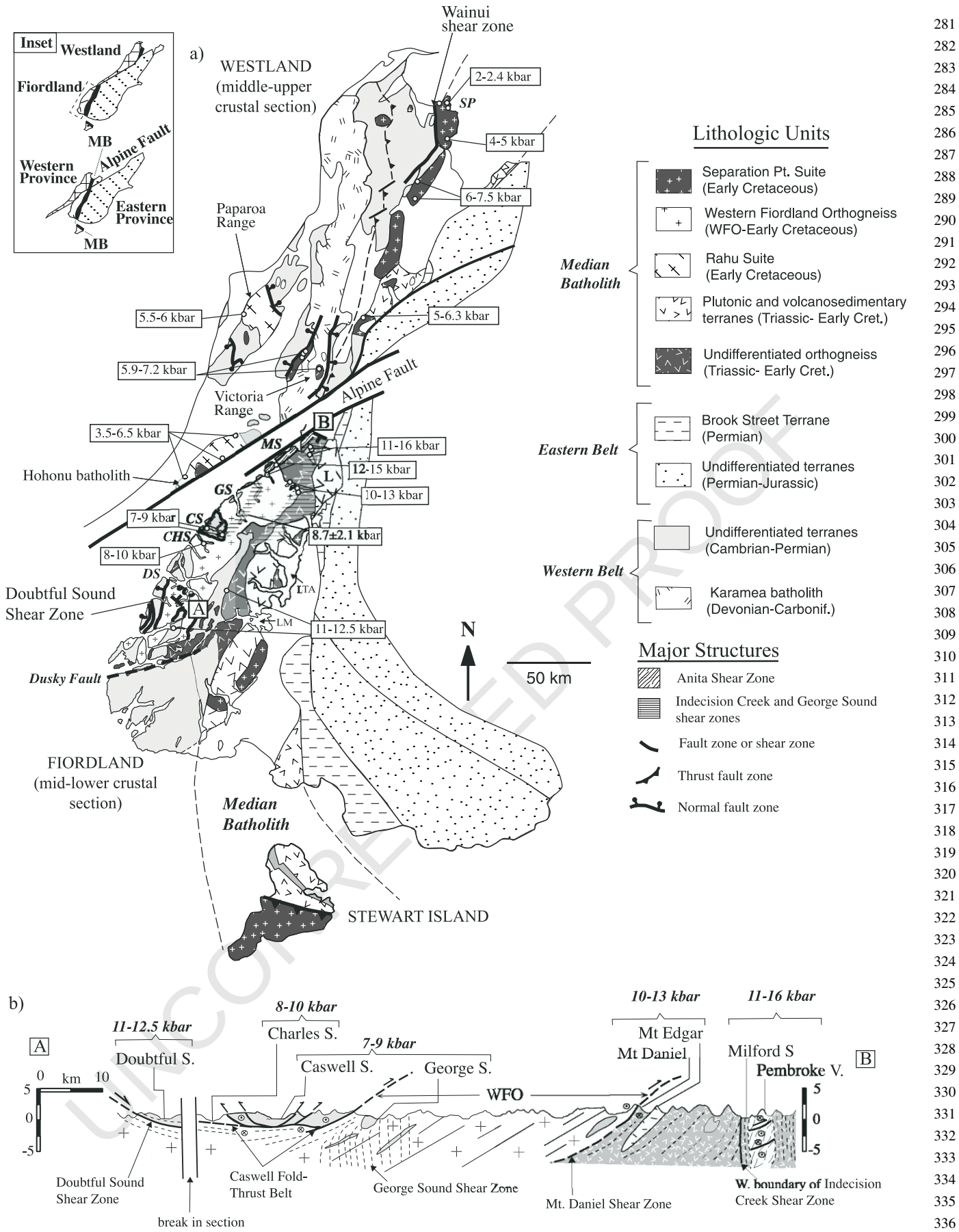

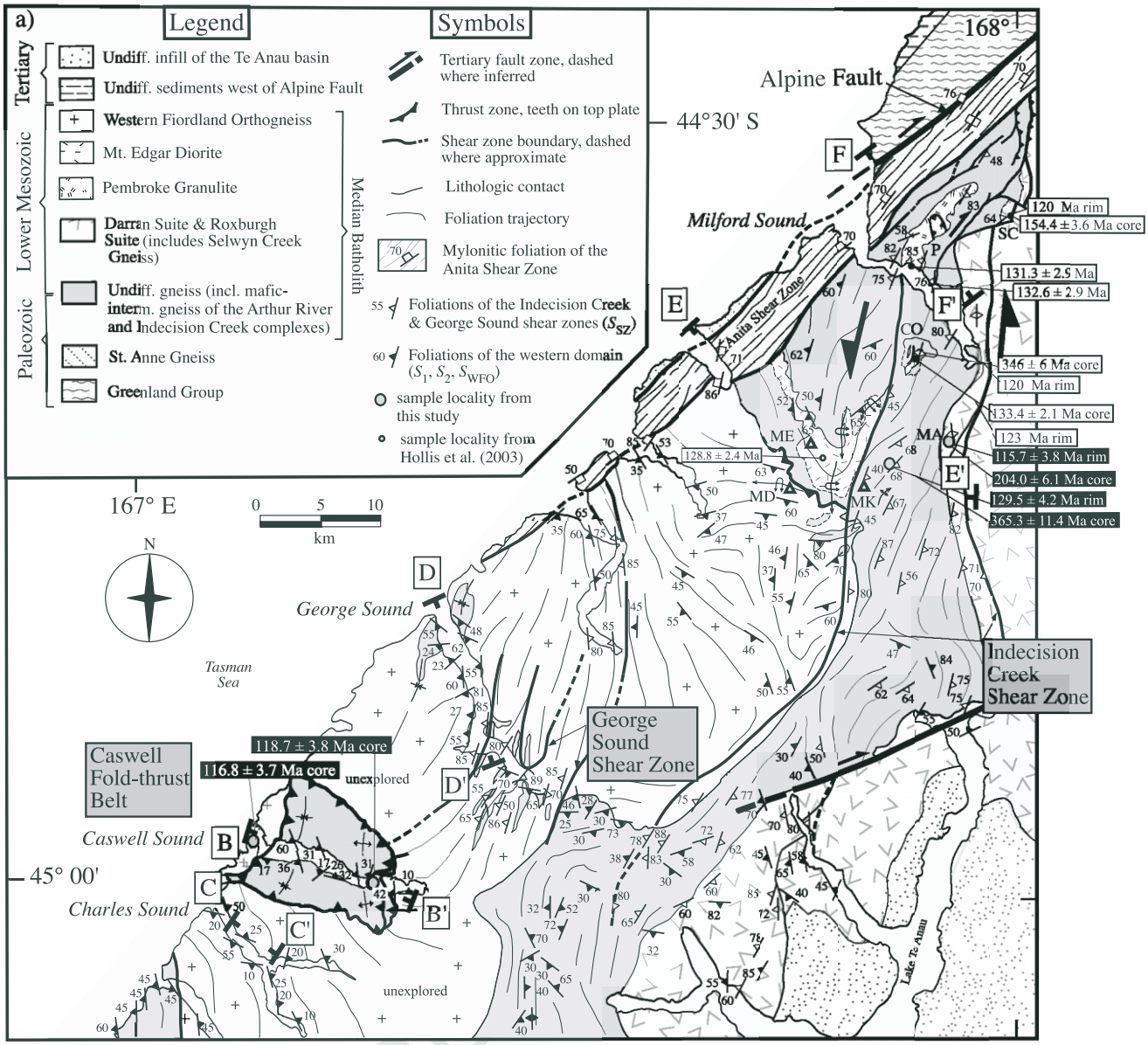

Fig. 2. Structural map of Fiordland. Only main lithologic divisions are shown (see Turnbull (2000) and Klepeis and Clarke (2003) for details). Bold black lines show boundaries of major shear zones. Structural measurements are from Bradshaw (1985, 1990), Blattner (1991), Klepeis et al. (1999), Daczko et al. (2002a), Claypool et al. (2002), Turnbull (2000) and Klepeis and Clarke (2003). Foliation trajectories (thin black lines) show interpolation of structural trends. Plotted U–Pb dates are from Hollis et al. (2003; white boxes) and this study (black boxes). Abbreviations show site localities: Mt. Daniel (MD), Mt. Edgar (ME), Camp Oven Creek (CO), the Pembroke Valley (P), Mt. Ada (MA), Selwyn Creek (SC), Mt. Kepka (MK).

(Williams and Harper, 1978; Mortimer et al., 1999a,b). Hollis et al. (2003) obtained ages that suggest this amalgamation occurred as early as ~136 Ma and certainly by ~129 Ma. Tulloch and Kimbrough (2003) determined that differences in composition and age reflect a configuration where mantle-derived plutons of the outboard belt were underthrust beneath Gondwana where they partially melted at high pressures producing magma of the inboard belt. Daczko et al. (2001a, 2002a) and Klepeis and Clarke (2003) describe the contraction that accompanied this amalgamation.

By ~108–105 Ma, regional extension affected parts of Fiordland and Westland (Bradshaw, 1989; Tulloch and Kimbrough, 1989; Gibson and Ireland, 1995; Spell et al., 2000). Extensional metamorphic core complexes in the Paparoa and Victoria ranges (Fig. 1) formed in the mid–upper crust beginning at this time. Emplacement of the ~110 Ma Hohonu granitoids (Fig. 1; Waight et al., 1998)

and the youngest plutons of the Separation Point Suite at ~105 Ma (Tulloch and Kimbrough, 2003) may have overlapped with the transition to extension. The Doubtful Sound Shear Zone (Gibson et al., 1988; Gibson and Ireland, 1995) and the Anita Shear Zone (Hill, 1995; Klepeis et al., 1999) record decompression and exhumation after ~108–105 Ma (Fig. 1).

During the Cenozoic changes in relative motions among the Pacific, Australian, and Antarctic plates led to the development of the modern Pacific–Australian plate boundary by ~25 Ma (Cooper et al., 1987; Sutherland, 1995; Lamarche et al., 1997). Approximately 70–75% of current motion arising from the oblique convergence between the Australian and Pacific plates is accommodated by slip along the Alpine Fault (Sutherland et al., 2000; Norris and Cooper, 2001). Claypool et al. (2002) review the effects of late Cenozoic faulting and exhumation (≤6 km) on the structure of northern Fiordland.

2.1. Early Cretaceous crustal thickening and magmatism in the mid–upper crust

In Westland, plutons of the ~126–105 Ma Separation Point Suite (Fig. 1) record Early Cretaceous emplacement depths of 8–27 km, with the greatest depths (17–27 km) occurring on the western side of the Median Batholith (Tulloch and Challis, 2000). The youngest plutons also occur on this western side (Tulloch, 1979; Harrison and McDougall, 1980; Kimbrough et al., 1994; Muir et al., 1994). Early Cretaceous deformation was distributed across a 50–75-km-wide zone in Westland. Plutons localized some of this deformation. Ductile shear zones, including the Wainui Shear Zone (Fig. 1), formed on the western side of the Separation Point Suite, including in its amphibolite facies contact aureole (Grindley, 1980; Bradshaw, 1993; Tulloch and Challis, 2000). Paleozoic fault zones also influenced Early Cretaceous deformation. A record of multiple displacements in many fault zones (Cooper, 1979) probably reflects some Mesozoic reactivation.

Crustal thickening by magma addition in the Eastern Belt is indicated by a peak in subduction-related magmatism at ~140 Ma (Tulloch and Kimbrough, 2003). A major thrust fault on Stewart Island (Fig. 1) formed between the outboard and inboard belts during ~125–105 Ma magmatism (Allibone and Tulloch, 1997; Tulloch and Kimbrough, 2003). Southeast of Fiordland, the Early Cretaceous Largs Terrane (L, Fig. 1; Williams, 1978; Mortimer et al., 1999b) is folded and thrust over the Brook Street Terrane (Bradshaw, 1989). In the Victoria Range (Fig. 1), argon thermochronology (Spell et al., 2000) and metamorphic data (Tulloch, 1979) suggest that thickening and burial of the Western Belt to mid-crustal levels initiated by ~130–120 Ma and occurred prior to ~105 Ma (Tulloch and Challis, 2000; Tulloch and Kimbrough, 2003).

2.2. Early Cretaceous crustal thickening, magmatism and partial melting in the mid–lower crust

In Fiordland, the WFO was emplaced into a mid–lower crust composed of Paleozoic metasediment and orthogneiss, and early Mesozoic intrusive rock (Hollis et al., 2003). Published ages from the WFO range from ~126 to ~116 Ma (Mattinson et al., 1986; Muir et al., 1998). New high-precision data reported by Tulloch and Kimbrough (2003) suggest that the main dioritic phase of the WFO was emplaced during the interval 126–124 ± 2 Ma. Hollis et al. (2004) reports zircon ion probe data from Mt. Daniel and George Sound that suggest that the WFO crystallized at 121.8 ± 1.7 and 120 ± 2.6 Ma, respectively, at these localities (Hollis et al., 2004). Part of the WFO near Doubtful Sound may be as young as ~116 Ma (Hollis et al., 2004). Tulloch and Kimbrough (2003) also report a 116.6 ± 1.2 Ma age from Wet Jacket Arm south of Doubtful Sound that supports this interpretation. Alternatively, the young zircon may reflect recrystallization.

Bradshaw (1989a, 1990) and Bradshaw and Kimbrough (1989) used metamorphic P–T paths to infer an up-pressure metamorphic history for the WFO following its emplacement. Clarke et al. (2000) confirmed an up-pressure loading history from $P < 8$ to 14–16 kbar for rocks of the Arthur River Complex on the basis of metamorphic mineral assemblages. The Arthur River Complex (Fig. 2) is composed of Paleozoic paragneiss and both Paleozoic and Mesozoic orthogneiss that lie below the WFO (Tulloch et al., 2000; Hollis et al., 2003).

Oliver (1990) and Brown (1996) inferred that the cause of burial involved magma loading during and following emplacement of the WFO. Muir et al. (1995, 1998) suggested that part of the Median Batholith was thrust to lower crustal depths beneath western Fiordland and melted to produce the WFO. This interpretation is supported by geochemical data reported by Tulloch and Kimbrough (2003). Daczko et al. (2002a) showed that some tectonic burial was accomplished by the stacking of thrust sheets above the WFO. Klepeis and Clarke (2003) showed that lower crustal thickening involved displacements on both steep and gently dipping shear zones.

Granulite facies metamorphism in the lower crust accompanied and followed WFO emplacement (Oliver, 1977; Bradshaw, 1985, 1989a,b; Gibson and Ireland, 1995; Clarke et al., 2000; Daczko et al., 2001b). Thin metamorphic overgrowths on Paleozoic and Mesozoic zircon yield an average age of ~120 Ma in northernmost Fiordland (Tulloch et al., 2000; Hollis et al., 2003). This age is interpreted to represent the peak of metamorphism at temperatures of 750 °C < T < 850 °C. Pressures representing the peak of this metamorphism range from $P = 7$–9 kbar in the shallowest part of the section to $P = 11$–16 kbar at the deepest levels (data plotted in Fig. 1). Recent work suggests that granulite facies metamorphism accompanied the partial melting of metadiorite during and

after WFO emplacement and was promoted by the mobilization of water-poor melt in fractures (Clarke et al., 2000; Daczko et al., 2001b). Partial melting was controlled by the decomposition of hornblende ± clinozoisite (Antignano, 2002; Klepeis et al., 2003). Antignano (2002) used experiments to show that positive volume changes associated with the reaction of hornblende ± clinozoisite to produce melt were sufficient to fracture matrix feldspar and quartz. Klepeis and Clarke (2003) outline relationships that suggest the fractures formed by high fluid pore pressure in melt pockets and propagation during the fluid-absent melting of mafic lower crust.

Following peak metamorphism at the granulite facies, the batholith and its lower crustal host rock hydrated and cooled (Daczko et al., 2002b). Quantitative cation mapping and thermodynamic modeling of kyanite- and paragonite-bearing assemblage by Daczko et al. (2002c) suggested isobaric cooling of the Arthur River Complex to conditions of $T = 650–700$ °C and $P = 11–15$ kbar.

3. Structure of the middle and lower crustal sections

Continuous exposure along Fiordland's waterways combined with ridge sections above the fjords were used to construct serial cross-sections from Milford Sound to Caswell Sound (Figs. 1b, 3 and 4). This approach allowed determination of the three-dimensional structure of northern Fiordland (Figs. 2 and 5). The results show a tilted middle–lower crustal section (~80 km horizontal distance) on the western side of Fiordland that includes both the upper and lower contacts of the WFO. The uppermost contact of this batholith is well exposed at Caswell Sound; the lowermost contact is well exposed at Mt. Daniel (Figs. 1b and 2). These contacts dip variably to the S and W and are deformed by shear zones of variable thickness and geometry. The shear zones at these two localities formed at different paleodepths and divide the crustal section into distinctive structural domains.

The geometry of the titled section, with Caswell and George sounds exposing the middle crust (25–30 km depth) and areas north of Mt. Daniel exposing the lower crust (45–50 km depth) is consistent with variations in Early Cretaceous paleodepths determined using published thermobarometric data (Fig. 1). Pressures reflecting the peak of Early Cretaceous (~120 Ma) metamorphism at Caswell and George sounds have a range of $P = 7–9$ kbar and occur within the WFO and its contact aureole (Daczko et al., 2002a). Pressures reflecting peak metamorphic conditions during and following emplacement of the WFO at Mt. Daniel and Milford Sound are $P = 10–13$ kbar (Bradshaw, 1985, 1989a,b) and $P = 12–16$ kbar (Clarke et al., 2000), respectively. South of Charles Sound the dip of the WFO-country rock contact changes to the NE, subparallel to the Doubtful Sound Shear Zone (Fig. 1b). Peak pressures in the WFO at Charles Sound are recorded at $P = 8–10$ kbar (Bradshaw, 1985; Brown, 1996). South of Charles Sound paleodepths increase. In the footwall of the Doubtful Sound Shear Zone, pressures reflecting the peak of Early Cretaceous metamorphism are $P = 11–12.5$ kbar (Gibson and Ireland, 1995). The tilted depth section between Caswell and Milford sounds thus lies in the hanging wall of the Doubtful Sound Shear Zone (Fig. 1b).

The western boundary of the lower crustal section in northern Fiordland coincides with the steep, upper amphibolite facies Anita Shear Zone (Fig. 2). This shear zone cuts all Early Cretaceous fabrics within the Arthur River Complex and the WFO (Figs. 2 and 5) and separates the high-grade rocks from Paleozoic rocks (including the Greenland Group and Saint Anne Gneiss) to the west. The western boundary of the lower crustal section coincides with the eastern margin of a 10–15-km-wide shear zone named the Indecision Creek Shear Zone by Klepeis and Clarke (2003). This shear zone separates the granulites from weakly metamorphosed ~150–130 Ma plutonic rock of the Darran and Roxburgh suites to the east (Fig. 2). Most of the Darran Suite is only weakly deformed except on its western sides (see also Blattner and Graham, 2000). Highly deformed rocks on this western side include the Selwyn Creek Gneiss (SC, Fig. 2). Brittle faults deform the steep margins of the Anita Shear Zone and the Darran Suite.

East of the Anita Shear Zone the lower crustal section displays two structural domains (Figs. 2 and 5) that are separated by a 4–5-km-wide transitional zone (Fig. 4a). The western domain is composed of Paleozoic metasediment, mafic dikes, and layered intrusions, including the ~129 Ma Mt. Edgar Diorite (Fig. 2; Hollis et al., 2003). Igneous layering and gneissic foliations in this domain dip moderately to the S, W and SW (Fig. 2). The eastern domain, collectively termed the Indecision Creek Complex by Bradshaw (1990), is dominated by steep foliations of the Indecision Creek Shear Zone (Figs. 2 and 4). This latter domain contains gabbroic gneiss, dioritic gneiss and deformed felsic dikes. In the transitional zone, the foliations of the western domain are folded and transposed parallel to the margins of the Indecision Creek Shear Zone. At George Sound, a 4–10-km-wide zone of high strain, named the George Sound Shear Zone by Klepeis and Clarke (2003), displays foliations that are similar in geometry to those of the Indecision Creek Shear Zone (Fig. 2). This shear zone lies structurally below a mid-crustal fold–thrust belt at the Caswell Sound (Fig. 2) that was first identified by Daczko et al. (2002a).

4. Shear zone evolution in the middle and lower crust

4.1. The Caswell Sound fold–thrust belt

At Caswell Sound, garnet granulite and upper amphibolite facies thrusts sole into a subhorizontal shear zone located at and below the contact between the WFO and its

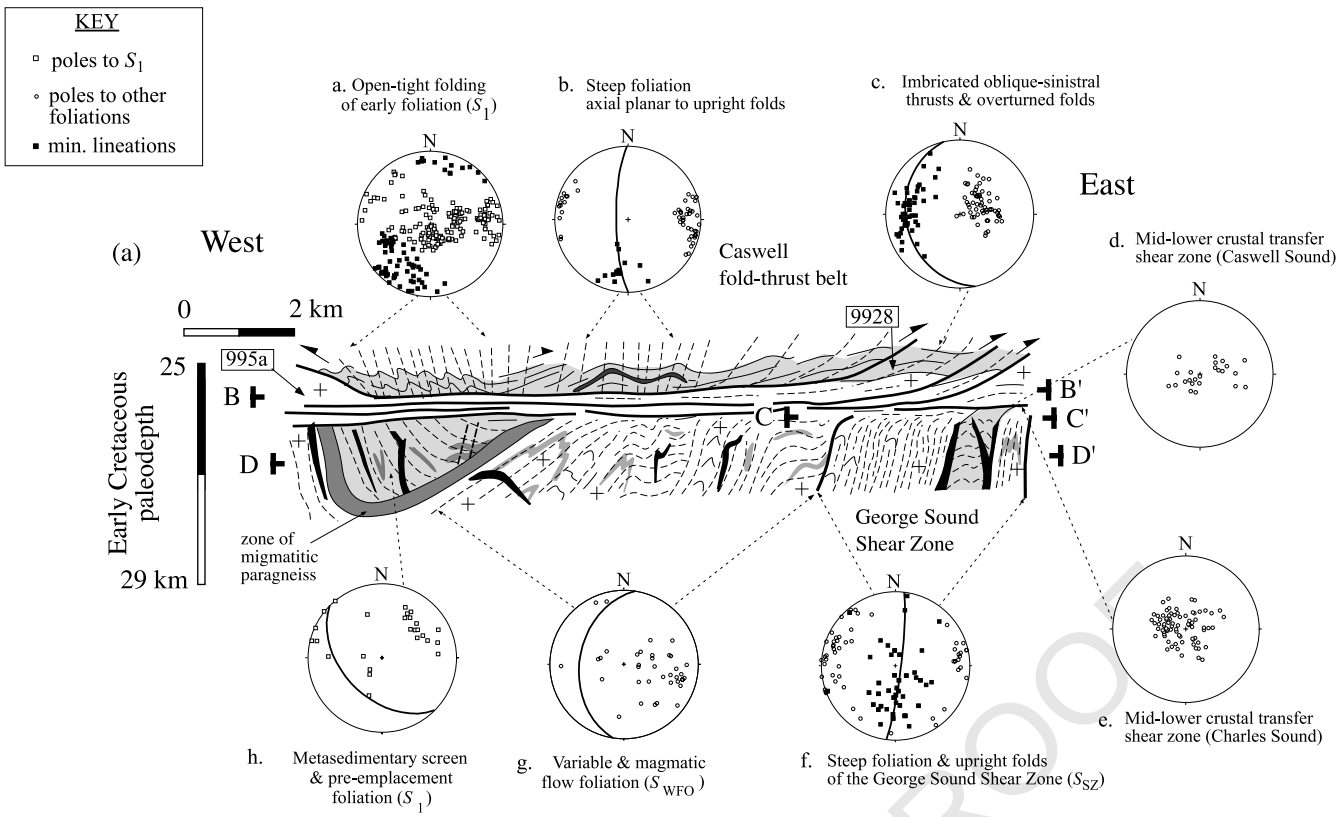

Fig. 3. Composite NW–SE profile of region between Charles Sound and George Sound. See Fig. 2 for section locations. Light shaded regions in B–B′ are metasedimentary (Paleozoic–Mesozoic) country rock. Shaded and black units in D–D′ are felsic and mafic dikes, respectively. Thin, solid, black lines are lithologic layering, dashed lines are foliation trends, and bold, black lines are shear zones. Equal area stereoplots (a–h) show poles to foliations, lineations and fold axes. All data were measured by the authors and Daczko et al. (2002a) except those in plot e, which are from Bradshaw (1985). Locations of samples (995a, 9928) for U–Pb analyses are shown. Sample 995a is from the Mckerr monzodiorite.

host rock (Fig. 3). Inside the WFO, the shear zone is defined by a ~1-km-thick section of subhorizontal to gently dipping upper amphibolite facies foliations (Fig. 3d and e). Country rock is composed of calcsilicate gneiss, marble, and metapsammitic schist that probably form part of the Paleozoic–Triassic sequences of Gondwana (Bradshaw and Kimbrough, 1991; Hollis et al., 2004). At the east end of the sound, imbricated, W-dipping thrust splays formed within the contact aureole of the WFO and locally cut across it (Fig. 3). Tight to isoclinal, S-plunging folds between thrusts deform a penetrative gneissic foliation (S_1) in metasedimentary country rock. To the west of the imbricate series the fold geometry changes from tight and overturned to open and upright, reflecting a decrease in strain intensity above and away from the WFO margin and the basal shear zone. A steep upper amphibolite facies foliation parallels the axial planes of the folds (Fig. 3b). Farther west (~12 km), the folds gradually tighten and overturn to the east above an E-dipping thrust fault. This E-dipping thrust separates the high-grade rocks of the thrust belt to the east from the weakly deformed McKerr monzodiorite to the west (Fig. 3).

Flattened clusters of coarse hornblende, clinozoisite and garnet in a feldspar matrix define thrust plane foliations inside the WFO. Inside the WFO and within 500 m of its uppermost contact, feldspar in the thrust zones was dynamically recrystallized along grain boundaries. In contrast, greater than 500 m above the contact, feldspar behaved in a brittle manner during deformation in thrust zones although mylonitic textures also are common. Thrust faults greater than 500 m and up to 2.5 km from the contact with the WFO are defined by aligned chlorite, muscovite, quartz, feldspar, clinozoisite and amphibole. Daczko et al. (2002a) described these variations in mineral assemblage in detail and showed that they reflect a temperature gradient of $T = 700–800$ °C within the (500 m thick) contact aureole and $T = 550–600$ °C outside of it. These strong links among increasing metamorphic grade, the recrystallization of feldspar, and proximity to the WFO suggests that the thrusts were preferentially partitioned into crust that was thermally softened by the emplacement of the batholith. The subsolidus character of the thrust fabrics also indicates that contraction outlasted emplacement and crystallization of the WFO.

Structurally below the Caswell thrusts, the WFO is composed of layered dioritic intrusions and folded rafts of upper amphibolite facies country rock (Fig. 3). At George Sound (Fig. 2) the rafts contain a folded layer-parallel foliation (S_1) that is cut by the dioritic intrusions and metasedimentary rock is migmatitic within 500 m of the

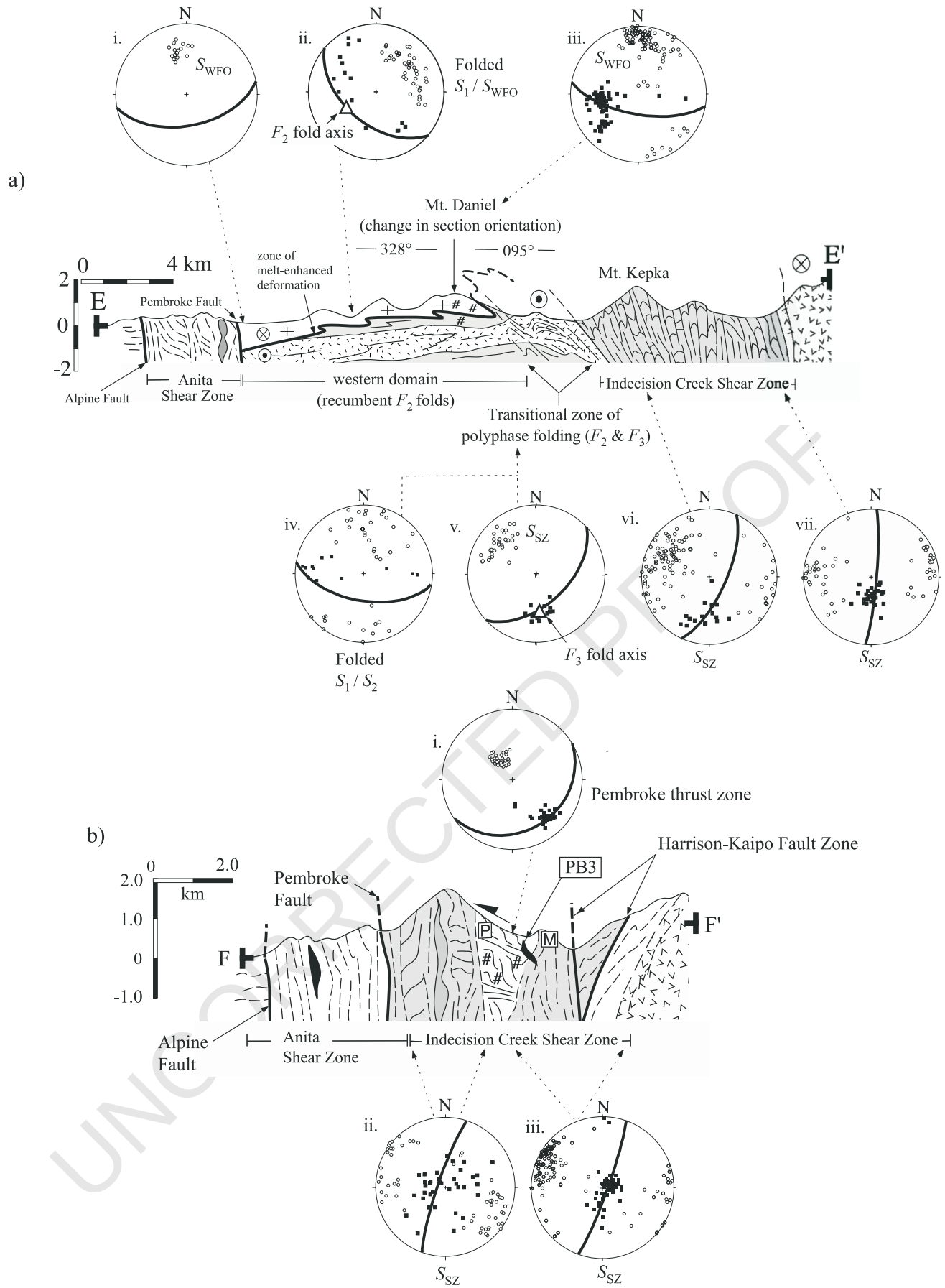

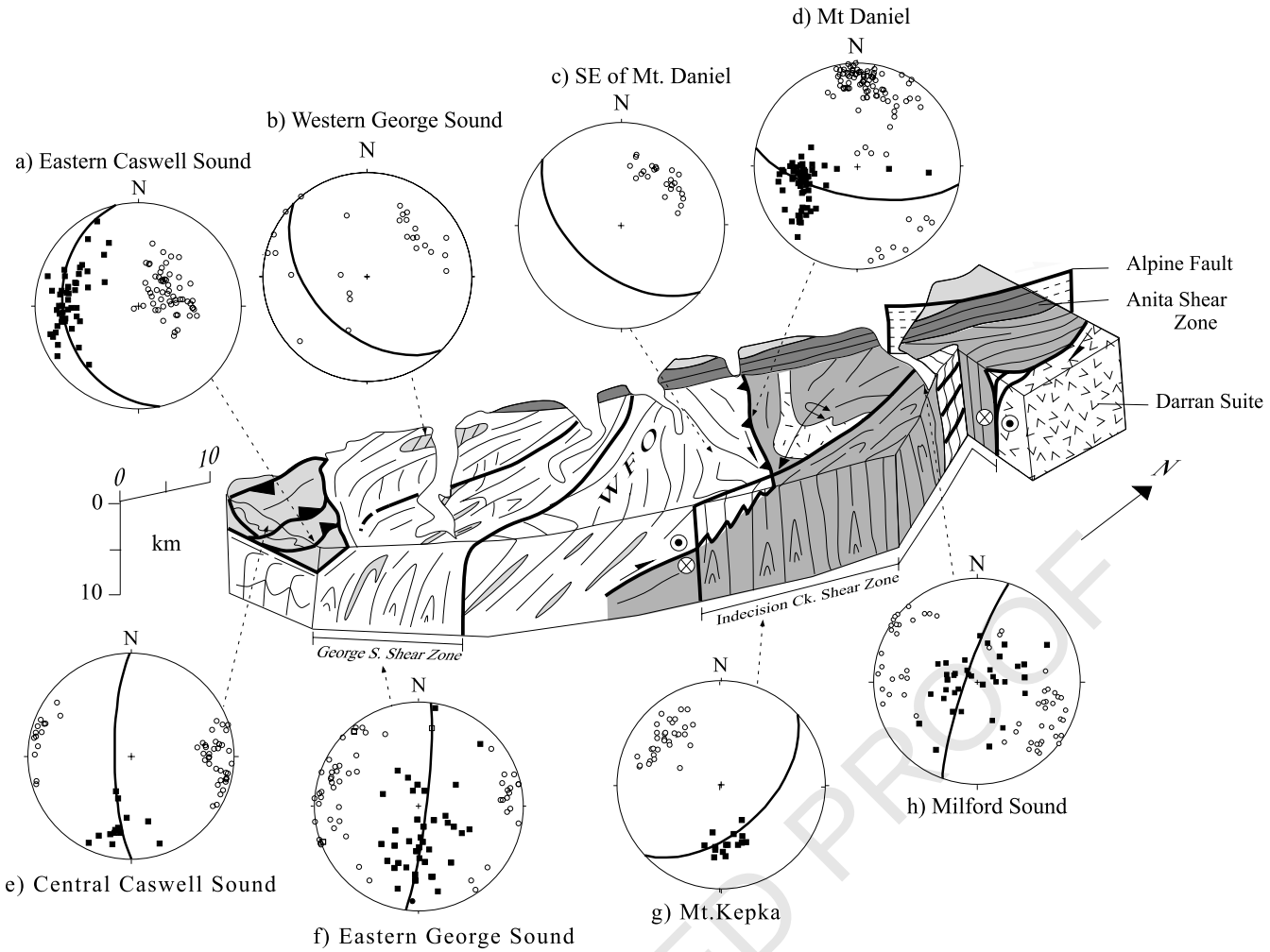

Fig. 5. Composite block diagram of region between Caswell Sound (south end) and Milford Sound (north end) constructed using structural relationships shown in Figs. 1a, 2, 3 and 4. Equal area stereoplots show poles to foliations, mineral lineations and fold axes. Plots (a)–(d) represent the western domain; plots (e)–(h) represent the eastern domain. Symbols the same as in Fig. 3. Plot (c) is from Bradshaw (1985). WFO is the Western Fiordland Orthogneiss.

WFO margin (Fig. 3). The preservation of this migmatite supports our interpretation that thrust zones were preferentially partitioned into a similar zone that was weakened by melt and heat at Caswell Sound. Foliations inside the diorite form two dominant structural trends. The first trend includes highly variable magmatic flow foliations (S_{WFO}) defined by the planar alignment of clinopyroxene, hornblende, tabular plagioclase and other minerals. The second trend includes steeply to moderately dipping subsolidus foliations (e.g. Fig. 3f and g) that are heterogeneously developed within the batholith. These latter foliations are best developed in the George Sound Shear Zone (Figs. 2 and 3f) where they cut the older synmagmatic S_{WFO} foliations. Tight, upright, S-plunging folds of dikes with steep axial planar foliations display geometries that are similar to the upright folds and steep foliations of the Caswell fold–thrust belt (compare Fig. 3b and f). The George Sound Shear Zone flattens up section and merges with the subhorizontal shear zone beneath the Caswell fold–thrust belt (Fig. 3).

4.2. The Mount Daniel Shear Zone

A few hundred meters above the lowermost contact of the WFO exposed at Mt. Daniel, the main phase of the WFO is a coarse-grained diorite that contains pods of gabbro. A hornblende cumulate layer occurs at the base of the diorite (Fig. 6). These rocks display primary igneous layering and, locally, a coarse-grained magmatic flow foliation (S_{WFO}) defined by aligned hornblende, clinozoisite, and plagioclase

Fig. 4. Cross-sections across the Mt. Daniel region (a) and north of Milford Sound (b). See Fig. 2 for locations. Equal area stereoplots show poles to foliations, lineations and fold axes. Symbols the same as in Fig. 3. Plots i, ii, and iv in (a) include data from Bradshaw (1985). P and M are samples of orthogneiss dated by Tulloch et al. (2000). PB3 in (b) is post-tectonic dike discussed in the text. # represent granulite facies fracture arrays.

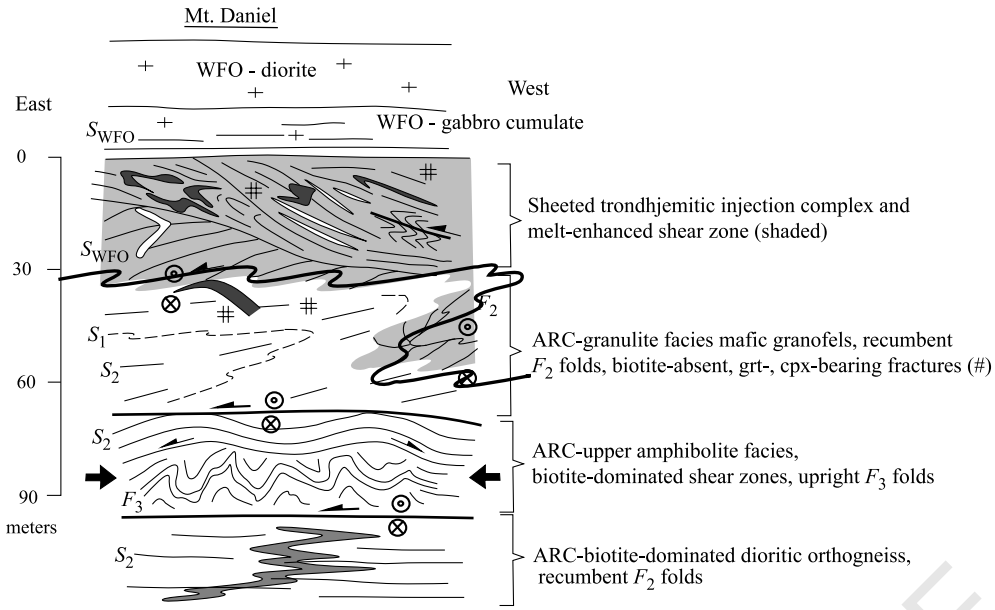

Fig. 6. Vertical profile of the Mt. Daniel Shear Zone. Bold lines are upper amphibolite facies shear zones discussed in the text. WFO is Western Fiordland Orthogneiss; ARC is Arthur River Complex. # represent granulite facies fracture arrays.

that parallel a moderately (40–50°) SW-dipping basal contact (Fig. 4a, part iii).

Below the cumulate layer is a banded igneous complex (Fig. 6) that preserves evidence of both suprasolidus and subsolidus deformation. Sheeted tonalite intrusions in this zone display undulate, diffuse contacts with slightly more mafic tonalitic bodies that reflect injection into an incompletely crystallized host (see also Fig. 5 of Klepeis and Clarke, 2003). Discordant mafic dikes with sharp, straight contacts cut some tonalite sheets and, in turn, are cut by veins that originate from the surrounding tonalite host. These mutually crosscutting relationships indicate the simultaneous emplacement of tonalitic and more mafic sheets.

The central and lower parts of the banded igneous complex preserve relationships indicating the accumulation of high strains while the rocks were partially molten. Migmatitic tonalite and trondhjemite sheets are complexly interfolded and stretched. Recumbent folds of dikes and igneous layering are common. Interfolded, transposed sheets are cut by less deformed sheets, indicating that deformation coincided with the periodic emplacement of the sheeted intrusions (see also Fig. 5d of Klepeis and Clarke, 2003). Tightly folded pegmatites display axial planes that parallel the margins of tonalite layers. However, despite the evidence of the high strains required to produce these tight folds, many of the pegmatite dikes are not foliated. Coarse biotite in the dikes forms radial or misaligned patterns and plagioclase exhibits a clean, interlocking igneous texture with little evidence of subsolidus recrystallization. These features define a thin melt-enhanced shear zone at the base of the WFO (Fig. 6).

Beneath the basal shear zone, metagabbroic–metadioritic orthogneiss forms part of the Arthur River Complex (Fig. 6). Greater than 100 m below the contact zone at Mt. Daniel, the dominant rock type is a biotite-rich dioritic orthogneiss. This latter unit is compositionally similar to the ~129 Ma Mt. Edgar Diorite (Fig. 2). Between the biotite orthogneiss and the basal shear zone is a 30–50-m-thick zone of granulite facies, garnet-rich metagabbro. The metagabbro contains little plagioclase and no biotite. These observations suggest that the metagabbro represents a depleted part of the Arthur River Complex that resulted from partial melting of a biotite-rich dioritic host similar to that which occurs below the metagabbro (see also Daczko et al., 2002b).

In addition to evidence of suprasolidus deformation, a heterogeneous subsolidus overprint also occurs within the basal shear zone. Thin (<10 m wide) upper amphibolite facies shear zones locally cut the margins of some folded intrusions and preserve evidence that plagioclase grain sizes were reduced during dynamic recrystallization. The shear zones parallel the axial planes of recumbent, SE-plunging folds that are geometrically similar to the melt-enhanced folds we described earlier. However, the former contain a weak axial planar foliation (S_2) defined by flattened plagioclase and aligned biotite and hornblende (Fig. 4a, parts ii and iv). The heterogeneous development of this subsolidus foliation and a lack of transposition during folding resulted in the preservation of the migmatitic features at the base of the WFO. In addition, the subsolidus folds deform the entire lower contact of the basal shear zone and form part of a set that also occurs at the base of the Mt. Edgar Diorite (Fig. 4a). We refer to these folds as F_2 structures because they deform primary igneous layering and older gneissic foliations (S_1). The presence of S_2 and the subsolidus shear zones indicate that F_2 folding either post-dated or outlasted crystallization of the melt-enhanced shear zone. We suggest that they are related to crustal thickening

during and slightly after emplacement and burial of the WFO.

Another set of folds occurs in a narrow zone (~20 m thick) between parallel minor shear zones in the Arthur River Complex (Fig. 6). These folds are disharmonic, mostly upright and plunge gently to moderately to the S (Fig. 4a, part v). A spaced crenulation cleavage approximately parallels the axial planes of these folds. This same style of folding occurs in the transitional zone between the western and eastern domains (Figs. 2 and 4a). On the basis of crosscutting relationships, we refer to these upright folds as F_3 structures (Fig. 4a, part v).

Finally, above and below the basal shear zone are arrays of discordant veins and fractures filled with leucosome that cut all ductile fabrics in the basal shear zone (# symbols in Figs. 4 and 6). Narrow (6–7 cm) dehydration zones containing garnet- and clinopyroxene-bearing assemblages surround garnet-bearing leucosome in some fractures. Inside these zones, hornblende–clinozoisite-bearing assemblages that define foliation in these rocks are replaced by garnet, clinopyroxene, and rutile. Daczko et al. (2002b) reported symplectic intergrowths of clinopyroxene and kyanite and also of clinozoisite, quartz, kyanite and plagioclase that partially replace the older hornblende and clinozoisite assemblage. These assemblages and reaction textures record dehydration of the WFO and its host rocks at the garnet granulite facies following cooling of the WFO and its basal shear zone at Mt. Daniel (Daczko et al., 2002b). None of the fractures or leucosome appears folded.

4.3. The Indecision Creek and George Sound Shear Zones

The Indecision Creek and George Sound Shear Zones (Figs. 2–4) display vertical to steeply dipping, upper amphibolite facies foliations (S_{SZ}) that strike to the N, NE and NNE and dip variably to the NW and SE. These steep foliations parallel the axial planes of tight, S-plunging folds. Steeply to gently plunging hornblende and plagioclase mineral lineations occur on foliation planes (Figs. 2–4). Rock fabrics are locally mylonitic and the folds and intrusive contacts are transposed in the shear zone.

South of Milford Sound, the transitional domain (Fig. 4a) preserves crosscutting relationships among shear zone fabrics and other fabrics and fold sets of northern Fiordland. In this zone, all igneous layering and gneissic foliations of the western domain (S_1, S_{WFO}, S_2) and F_2 folds are tightly folded into south-plunging F_3 folds (Figs. 2 and 4a). From W to E across this zone, F_3 fold axial planes steepen to near vertical, interlimb angles decrease, and the F_3 folds gradually are transposed parallel to the steep S_{SZ} foliations (Fig. 4a, parts v, vi and vii). The dominant S_{SZ} foliation parallels the axial planes of these tight F_3 folds. These changes define a 3–4-km-wide positive strain gradient that increases from W to E into the central part of the shear zone.

North of Milford Sound, in the Pembroke Valley (P, Fig. 2), steep fabrics of the Indecision Creek Shear Zone envelop a large lens of dioritic and gabbroic gneiss (Fig. 4b). This locality preserves features that record the progressive development of mineral assemblages and fabrics in the Indecision Creek Shear Zone. One of the most spectacular features is a lattice-like array of 3–5-cm-wide dehydration zones that surround steep, orthogonal sets of leucosome-filled fractures in dioritic and gabbroic orthogneiss. The dehydration zones contain coronas of garnet and clinopyroxene mantling hornblende. These reactions zones, like those found at Mt. Daniel and elsewhere, record dehydration at the garnet granulite facies. Descriptions of the petrology, P–Tconditions ($P = 13$–16 kbar, $T > 750$ °C), and origin of these features are provided by Blattner (1976), Oliver (1977), Bradshaw (1989a,b), Clarke et al. (2000) and Daczko et al. (2001b).

The dehydration zones and vein sets form markers (Fig. 7a) that record the evolution of two sets of superposed shear zones (Daczko et al., 2001a). The first set includes pairs of thin, 1–3-m-wide sinistral and dextral shear zones (Fig. 7b). The sinistral set is dominant and displays a steep mylonitic foliation that strikes to the E and NE. The dextral set is subordinate in size and abundance to the sinistral set. This latter set dips gently to moderately to the SW. Both shear zone sets contain gently plunging hornblende and clinozoisite mineral lineations. Superimposed on the sinistral and dextral shear zone pairs is a younger set of vertically stacked, layer-parallel shear zones that dip gently to the SE (Fig. 4b, part i and Fig. 7c). Each of these shear zones contains a 7–10-m-thick central zone where asymmetric pods of coarse-grained gneiss is surrounded by thin (<1 m thick) mylonitic to ultramylonitic shear bands. The asymmetric pods form imbricated, antiformal stacks. The thin shear bands locally dip steeply to the NW and SE and swing into parallelism with the gently SE-dipping shear zones located above and below them. Hornblende mineral lineations on foliation planes plunge to the SE (Fig. 4b, part i). The vertical spacing between parallel shear zones is ~50–100 m. The exact thickness of the stack is unknown.

East and west of the Pembroke Valley, the delicate dehydration zones and the layer-parallel thrusts are mostly transposed and recrystallized by the Indecision Creek Shear Zone (Fig. 7d). This shear zones cuts the lower (eastern side) contact of the WFO southeast of Mount Daniel (Figs. 2b, 4a and 5) and records retrogression of granulite facies mineral assemblages to the upper amphibolite facies. Southeast of the Indecision Creek Shear Zone, the George Sound Shear Zone cuts across the central part of the WFO (Figs. 2 and 3).

5. Kinematic relationships

The kinematics of deformation that occurred while the WFO batholith was partially molten are recorded best in the melt-enhanced basal shear zone exposed at Mt. Daniel. Oblique foliations and the truncation of sheeted intrusions

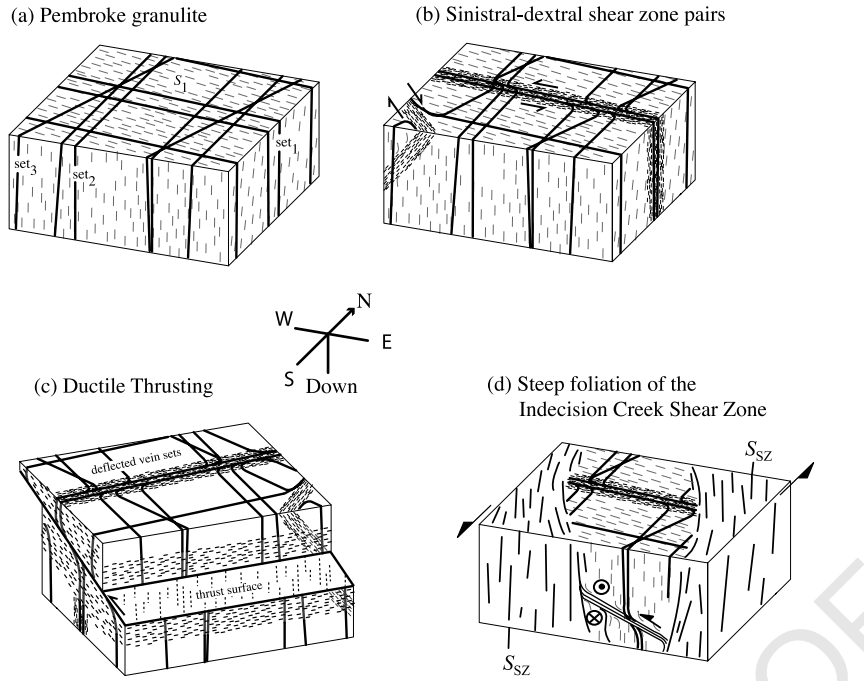

Fig. 7. Block diagrams showing the sequence of deformation recorded in structures at Pembroke Valley (modified from Fig. 3 of Clarke et al. (2000) and Fig. 13 of Daczko et al. (2001a)). (a) Garnet granulite facies fracture arrays cut S_1. (b) Steep, sinistral–dextral shear zone pairs deform fracture arrays. (c) Gently SE-dipping thrust zones (see also Fig. 4b) cut sinistral shear zones. (d) Steep upper amphibolite facies foliation (S_{SZ}) envelops shear zones at Pembroke Valley.

by successive sheets indicate top-to-the-E and -NE, thrust-style displacements parallel to W- and SW-plunging mineral lineations (Fig. 4a, part iii). The plunges of the lineations indicate a sinistral component to the deformation. The subsolidus shear zones that parallel the axial planes of F_2 folds give identical oblique-thrust senses of shear.

Below the WFO, kinematic indicators in the steeply dipping shear zone pairs of the Pembroke Valley (Fig. 7b) include oblique foliations, micro-faulted garnet, and asymmetric tails on feldspar porphyroclasts. These shear zones record mostly NE–SW stretching parallel to the arc with a component of sinistral displacement. Daczko et al. (2001a) showed that they also record subhorizontal shortening at high angles to the trend of the Median Batholith. The Pembroke Thrust Zone (Fig. 7c) contains asymmetric hornblende and clinozoisite fish, minor shear bands, and asymmetric tails on feldspar clasts that record a top-to-the-NW sense of shear. The style of displaced, asymmetric pods that are stacked on top of one another also reflects a component of layer-perpendicular thickening. Together, the steep shear zone pairs and Pembroke Thrust Zone record subhorizontal (layer-parallel) shortening normal to the batholith, sinistral arc-parallel displacements, and vertical (layer-perpendicular) thickening. This result is consistent with the oblique-thrust style displacements recorded in the melt-enhanced shear zone at Mt. Daniel, suggesting that this style of deformation began during emplacement of the WFO.

Above the WFO, the Caswell fold–thrust belt also records arc-normal contraction and crustal thickening following crystallization of the WFO. Lineation trends are similar to those that characterized those in the basal shear zone at Mt. Daniel (Fig. 5a and d). The spread of lineation plunges on foliation planes (Fig. 3c) also suggests that the imbricated thrusts record a component of sinistral displacement. The conjugate style of W-dipping thrusts with an E-dipping back thrust (Fig. 3) indicates compression directions at high angles to the trend of the arc.

Below the Caswell Sound fold–thrust belt, the Indecision Creek Shear Zone records shortening at high angles to the arc leading to the development of steep foliation planes. This shortening is best illustrated by the progressive change in fold geometry, including tightness and the steepening of fold axial surfaces, from W to E across the transition zone. Outcrop-scale sense of shear indicators, including hornblende and clinozoisite fish, asymmetric tails of biotite and hornblende around garnet porphyroblasts, asymmetric boudinage, and minor shear zones, mostly occur in areas of low–intermediate strain at the eastern and western edges of the shear zone. The sense of shear in these areas is dominantly sinistral parallel to gently and moderately plunging mineral lineations.

In the central part of the Indecision Creek Shear Zone, changes in orientation of hornblende lineations with increasing strain provide additional kinematic information. From W to E across the transition zone, the lineations change from gently and moderately S-plunging to near vertical and steeply plunging (compare Fig. 4a, parts vi and vii). The migration of these mineral lineations toward the dip line of the steep shear zone indicates stretching parallel

to this direction (Lin et al., 1998; Jiang and Williams, 1998). The reference frame provided by the gneissic layering of the western domain and well-defined boundaries indicate that the shear zone was thickening vertically during contraction.

The kinematic evolution of the George Sound Shear Zone has not been studied in detail due to its remote locality. However, the increase in fold tightness and rotation of hornblende lineations to down dip with increasing strain suggest that it also records arc-normal contraction, near vertical stretching. Minor shear zones show both dextral and sinistral displacements. Given that these styles are similar to those of the Indecision Creek Shear Zone (Fig. 5) we suggest that the kinematic evolution of the two shear zones is similar also.

6. The ages of lower crustal deformation, magmatism, and metamorphism

Published dates and four new age determinations were used to estimate the age of high-grade fabrics and intrusions. At Caswell Sound, U–Pb spot analyses on single zircons from the McKerr monzodiorite (sample 995a, Figs. 2 and 3) and from a dioritic dike within the zone of imbricated thrusts (sample 9928, Figs. 2 and 3) allowed us to place a lower limit on the age of deformation within eastern and western parts of the fold–thrust belt. Twenty analyses were conducted on the cores of zircon from sample 995a using a beam diameter of 50 microns (analytical procedures are described in Appendix A). Nineteen grains yielded analyses that are apparently of the same $^{206}Pb/^{238}U$ age, and one additional grain is discordant due to inheritance (Fig. 8a). The weighted mean of these analyses yields an interpreted crystallization age of 116.8 ± 3.7 Ma at the 2σ level (Fig. 8a and b). Twenty-two analyses were conducted on the cores of zircon grains from sample 9928 using a slot diameter of 50 microns. Twenty grains yield analyses that are apparently of the same age, and two additional analyses are apparently discordant due to a slight amount of inheritance. The final $^{206}Pb/^{238}U$ age is 118.7 ± 3.8 Ma (2σ level; Fig. 8c and d). These data suggest that the Caswell Sound fold–thrust belt evolved during and after the interval 122.5–113 Ma.

Two samples of syntectonic dikes from within the Indecision Creek Shear Zone (Ada2 and 0221K, Fig. 2) provided an approximate lower age limit of deformation in the shear zone. Forty-five analyses were conducted on zircon cores from sample Ada2 using a laser beam diameter of 25 microns. This dike from Mt. Ada (MA, Fig. 2) cuts the steep foliation (S_{SZ}) of the shear zone and also is folded within it. These analyses yield two clusters of ages (Fig. 8e and f). The older age of 204.0 ± 6.1 Ma from zircon cores is interpreted to record igneous crystallization. The rim ages of 115.7 ± 3.8 Ma are interpreted to record the growth of metamorphic zircon. The spread of the rim ages indicate that shear zone deformation continued through the interval 119.5–112 Ma.

Fifty analyses were conducted on zircon grains from sample 0221K using a beam diameter of 25 microns. This dike (from near Mt. Kepka, Fig. 2) also cut steep foliation planes (S_{SZ}) in the Indecision Creek Shear Zone and is folded within it. Most analyses were conducted on core areas of the zircon grains, with a smaller number of analyses on the rims (tips) of the grains. The rim analyses generally yield ages that are younger than the core ages. The occurrence of two distinct clusters of ages (Fig. 8g and h) suggests that the grains record two phases of zircon growth: an older phase at 365.3 ± 11.4 Ma that reflects crystallization of the dike, and a younger phase at 129.5 ± 4.2 Ma that reflects the growth of metamorphic zircon. The young rim ages obtained from the 0221K and Ada2 samples are in agreement with crosscutting relationships indicating that deformation in the Indecision Creek Shear Zone outlasted emplacement of the WFO.

These new ages are compatible with other published ages (Fig. 8i). Tulloch et al. (2000) identified Paleozoic (355 ± 10 Ma) oscillatory-zoned cores and Early Cretaceous (134 ± 2 Ma) sector-zoned cores from the Arthur River Complex. Both these core types displayed thin low-U rims that yield an average age of ~120 Ma but some with ages as young as ~105 Ma (Tulloch et al., 2000). Similar rim ages (Fig. 2) have been obtained from the deformed western margin of the Darran Suite (Selwyn Gneiss of Hollis et al., 2003). The Jurassic core age of sample Ada2 is compatible with similar ages obtained from the Darran Suite (Muir et al., 1998; Blattner and Graham, 2000). The rim age of sample 0221K is similar to ~136–129 Ma crystallization ages from intrusive rocks in the Arthur River Complex (Fig. 2; Hollis et al., 2003). Metamorphism leading to zircon growth also could have accompanied emplacement of intrusive rocks prior to the WFO (see also Tulloch et al., 2000).

Zircon ages of ~82 Ma from a post-tectonic dike (PB3; Fig 4b) indicate that ductile deformation in northernmost Fiordland terminated in the Late Cretaceous (Hollis et al., 2003). This age of a few million years younger than K–Ar ages on hornblende (Nathan et al., 2000) and U–Pb dates on apatite (Mattinson et al., 1986) indicate that the Arthur River Complex had cooled to $T = 300–400$ °C by ~90 Ma. Near Doubtful Sound, Gibson and Ireland (1995) dated thermal conditions of $T > 800$ °C at 107.5 ± 2.8 Ma from a sample of the WFO deformed by the Doubtful Sound Shear Zone (sample D in Fig. 8i). This age could reflect the recrystallization of zircon in the shear zone. However, the chemistry and age of the zircon suggested to Gibson and Ireland (1995) that it represents a new generation of zircon growth during metamorphism. The age is consistent with regional geologic relationships indicating that extension began by ~108–105 Ma (Tulloch and Kimbrough, 1989, 2003; Gibson and Ireland, 1995; Spell et al., 2000). K–Ar cooling ages of ~93 and ~77 Ma on amphibole and biotite,

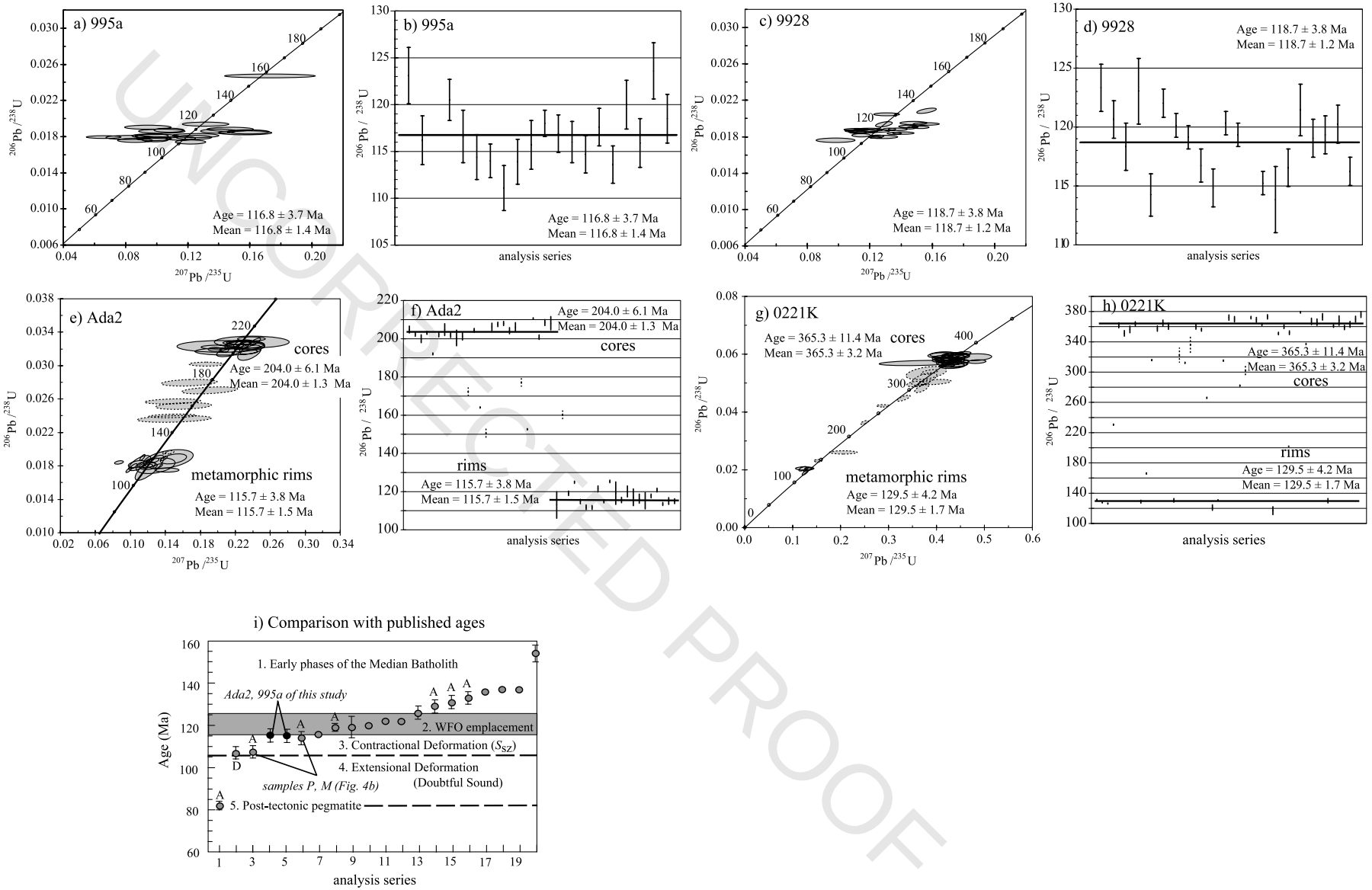

Fig. 8. U–Pb isotopic data from zircon collected using an inductively coupled plasma mass spectrometer (ICPMS). Plots (a), (c), (e) and (g) are concordia plots (ellipses shown with dashed lines were not used to calculate mean ages). An explanation is provided in Appendix A. Plots (b), (d), (f) and (h) show error analyses and distribution of analyses (solid lines) used to calculate mean ages and errors (2σ level). Locations of samples are shown in Fig. 2. Part (i) shows a comparison with published ages from Mattinson et al. (1986), Muir et al. (1998), Tulloch et al. (2000) and Hollis et al. (2003). Ages representing early phases of the Median Batholith are from both the Darran Suite and the Arthur River Complex (A). Samples P and M are from Tulloch et al. (2000) located in Fig. 4b. Post-tectonic dike is sample PB 3 reported by Hollis et al. (2003) and shown in Fig. 4b. Sample D is a zircon age from the extensional Doubtful Sound Shear Zone (Gibson and Ireland, 1995).

respectively, also support a late Cretaceous age for the Doubtful Sound Shear Zone (Gibson et al., 1988).

7. Correlation of structures within Northern Fiordland

Crosscutting relationships, geochronology, similarities in style and metamorphic grade, and the results of physically tracing structures above and below the WFO allowed us to correlate fabrics between Milford and Caswell Sounds. We use these correlations to reconstruct the sequential evolution of the section (Table 1, Figs. 9 and 10).

One especially useful marker unit is the WFO. The regional extent of this batholith and its ~126–120 Ma age allowed us to divide structures into groups that predated, accompanied, and post-dated its emplacement. Structures that predate emplacement occur in Paleozoic and early Mesozoic host gneiss located above and below the WFO or as xenoliths within it. Primary igneous layering and the gneissic foliations (S_1) in the Arthur River Complex and Darran Suite are included in this group (Table 1). These structures are locally cut by the WFO and mostly occur in the western domain (Figs. 2 and 4a).

The second group of structures includes all magmatic foliations (S_{WFO}) that formed within the WFO during its emplacement, including the Mt. Daniel Shear Zone (Table 1). These structures all exhibit evidence of deformation while the batholith was still partially molten. The links among increasing metamorphic grade, feldspar recrystallization, and proximity to the WFO also suggest that deformation in the Caswell Sound fold–thrust belt began during this stage. We include in this group the recumbent F_2 folds and axial planar foliations (S_2) that formed at the lower contact of the WFO.

In northernmost Fiordland the melt-induced fracture arrays and dehydration zones record the peak of granulite facies metamorphism in the lower crust during or immediately after WFO emplacement. The development of these arrays across large areas of the section (Pembroke Valley, Mt. Daniel, George Sound, Doubtful Sound) suggests that similar processes controlled their development. However, these features may exhibit slightly different ages across the section. Metamorphic rims on zircon suggest that in the Milford Sound region this metamorphism mostly occurred between ~123 and ~116 Ma with a clustering at ~120 Ma (Tulloch et al., 2000; Hollis et al., 2003; this study). Near Doubtful Sound a zircon age of 107.5 ± 2.8 Ma may indicate that granulite facies metamorphism there is younger (Gibson and Ireland, 1995). Despite this age range, we correlate these distinctive garnet granulite reaction zones (GRZ, Table 1). The recrystallization of these features in the Indecision Creek and George Sound shear zones indicates that they formed prior to the shear zones north of Caswell Sound.

The third group of fabrics includes the sinistral–dextral shear zone pairs (Fig. 7b), the Pembroke thrust zone (Fig. 7c), and the steep fabrics of the Indecision and George Sound Shear Zones (Fig. 7d). On the basis of structural relationships exposed in the Pembroke Valley, Clarke et al. (2000) and Daczko et al. (2001a) referred to the shear zone

Table 1
Time–space correlation of structures (dashed lines) from SW (left) to NE (right) within northern Fiordland. GRZ is garnet granulite reactions zones, S is foliation where subscript refers to rock unit and generation: WFO is Western Fiordland orthogneiss

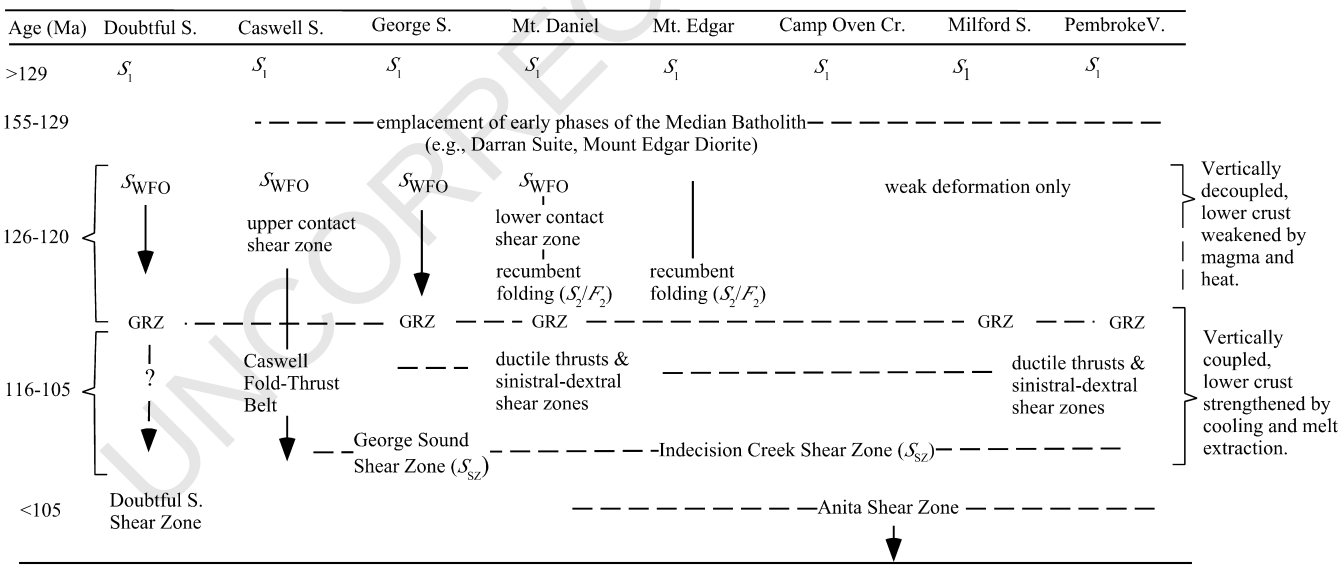

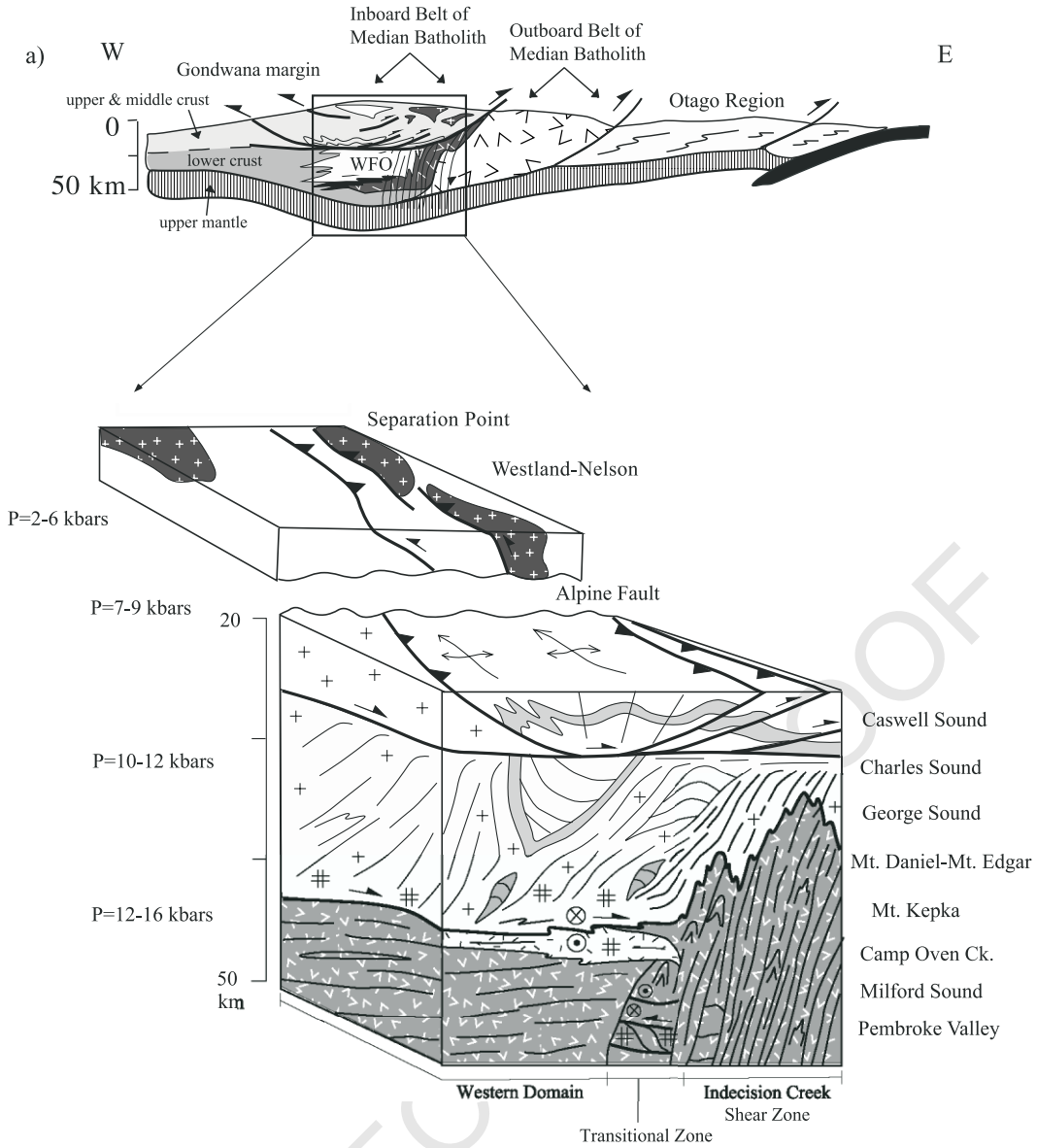

Fig. 9. (a) Interpretive cross-section showing the setting of the Fiordland–Westland orogen during the period ~126–105 Ma (modified from Klepeis et al., 2003). (b) Block diagram showing correlations of structures in Fiordland and Westland. Diagram was constructed using pre-Cenozoic configuration of the orogen and the relative structural position of the Fiordland cross-sections shown in Figs. 1b, 3, 4 and 5 (localities listed on right side of diagram). Section representative of Westland is from the north shore of Westland (separation point). Paleodepths were calculated from data shown in Fig. 1. Symbols (#) represent garnet granulite facies fracture arrays.

pairs and the ductile thrust fabrics as D_3 and D_4 structures, respectively. However, the occurrence of these features in the transitional zone of the Indecision Creek Shear Zone and evidence of arc-normal contraction during each phase of deformation suggest that they all reflect slightly different stages of the same contractional event. We also include in this group the tight F_3 folds. This correlation is consistent with crosscutting relationships indicating that all minor shear zones and the F_3 folds in the transitional zone deform S_1, S_2, F_2, S_{WFO} and GRZ structures. These relationships and the rim ages obtained from sample Ada2 (Figs. 6g and 8e) indicate that this deformation occurred after ~120 Ma and outlasted the emplacement of a ~116 Ma dike.

South of George Sound, the George Sound Shear Zone merges with the subhorizontal shear zone exposed at Caswell and Charles Sounds (Figs. 3 and 5). On the basis of crosscutting relationships with respect to the WFO both the Caswell fold–thrust belt and the George Sound Shear Zone developed following crystallization of the WFO and before the onset of regional extension (Table 1). Hollis et al. (2004) reports metamorphic rims on zircon from George Sound (an average age of ~120 Ma with ages spread across the interval ~138–106 Ma) that support this interpretation. Together, the combined isotopic data from Tulloch et al. (2000), Hollis et al. (2004) and from samples 995a, 9928 and Ada2 indicate that the Caswell fold–thrust belt and the

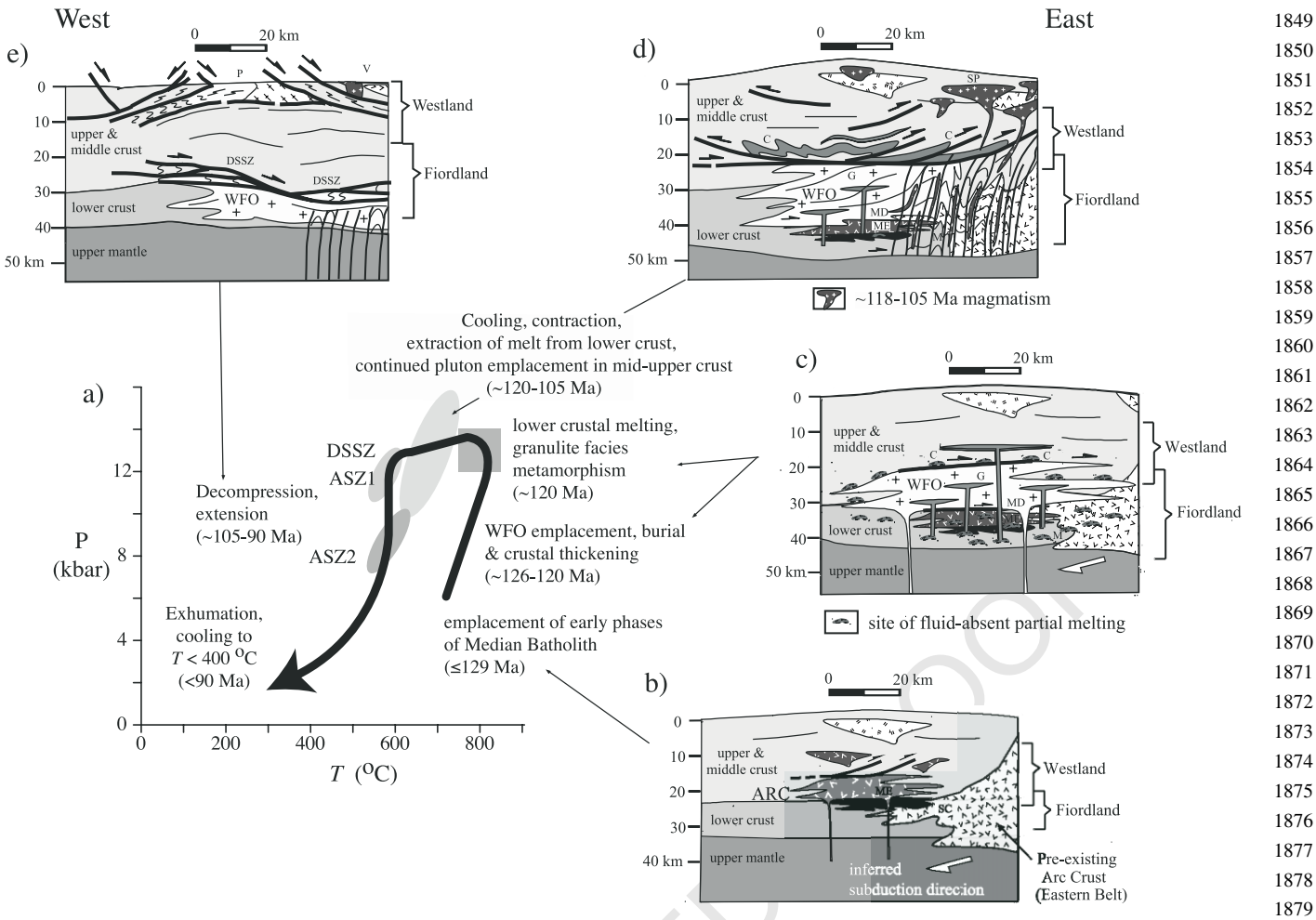

Fig. 10. Pressure–temperature–time path (a) for the lower crust exposed between Caswell and Milford sounds (modified from Daczko et al., 2002c). P–T data are compiled from Bradshaw (1985, 1989a,b), Gibson and Ireland (1995), Klepeis et al. (1999), Clarke et al. (2000) and Daczko et al. (2001a,b, 2002a,b,c). Shaded regions incorporate errors for specific metamorphic mineral assemblages discussed by Daczko et al. (2002c). Block diagrams ((b)–(e)) illustrate four stages in the tectonic evolution of the Fiordland–Westland belt. Patterns are the same as those in Fig. 1a. Parts (c)–(e) are modified from Klepeis et al. (2003). Abbreviations are: ASZ—Anita Shear Zone, ARC—Arthur River Complex, WFO—Western Fiordland Orthogneiss, ME—Mt. Edgar, SC—Selwyn Creek, C—Caswell Sound, G—George Sound, MD—Mt. Daniel, DSSZ—Doubtful Sound Shear Zone, P—Paparoa Range, V—Victoria Range.

Indecision Creek and George Sound Shear Zones all evolved during the interval ~122.5–105 Ma.

The last group of structures includes the Anita Shear Zone (ASZ, Figs. 5 and 9b; Table 2) and the Doubtful Sound Shear Zone (Table 1). Both shear zones record the exhumation (Fig. 9b) of the lower crust after ~108–105 Ma (Mattinson et al., 1986; Gibson et al., 1988; Nathan et al., 2000; Claypool et al., 2002). The Anita Shear Zone also preserves fabrics (including ASZ1 at $P = 12$ kbar and ASZ2 at $P = 8$ kbar, Fig. 10) that record Late Cretaceous–Cenozoic decompression (Klepeis et al., 1999).

8. Interpretation of vertical coupling and decoupling within the crustal column

The results of our analyses show that deformation accompanying the ~126–120 Ma emplacement of the WFO was localized within and at its upper and lower contacts (Figs. 1b, 9b and 10c). In contrast, deformation a few kilometers below the WFO during this period was weak to nonexistent (Table 1). The two layer-parallel shear zones at Mt. Daniel and Caswell Sound both separate areas of melt-enhanced deformation inside the WFO (S_{WFO}) from areas outside it where older structures (S_1 and igneous layering) and mineral assemblages are well preserved. In addition, structural relationships above and below the Mt. Daniel Shear Zone at the base of the WFO are discordant. This discordance and evidence that the structures above and below the basal shear zone formed at different times and under different physical conditions suggest that the crust above and below the lower contact of the WFO was decoupled during emplacement of the batholith.

As the batholith cooled and crystallized, the role of the layer-parallel shear zones began to change. The development of melt-induced fracture arrays and dehydration zones (Fig. 10c) that cut the lower contact of the WFO mark the abandonment of the melt-enhanced shear zone at Mt.

Table 2
U–Pb isotopic data

Sample	U (ppm)	$^{206}Pb/^{204}Pb$ ratio	$^{206}Pb/^{238}U \pm$ ratio (%)	$^{207}Pb/^{235}U \pm$ ratio (%)	$^{206}Pb/^{207}P \pm$ ratio (%)	Error correction	$^{206}Pb/^{238}U \pm$ age (Ma)	$^{207}Pb/^{235}U \pm$ age (Ma)	$^{206}Pb/^{207}Pb \pm$ age (Ma)	^{207}Pb correction $\pm$ age (Ma)
28-1c	*40*	*NA*	*0.0205 ± 0.5*	*0.1308 ± 5.8*	*21.579 ± 5.8*	*0.09*	*130.6 ± 0.7*	*124.8 ± 6.8*	*15 ± 70*	*131.0 ± 0.8*
28-2c	33	*NA*	0.0195 ± 0.7	0.1491 ± 4.7	18.022 ± 4.6	0.16	124.4 ± 0.9	141.1 ± 6.1	432 ± 51	123.3 ± 1.0
28-3c	42	*NA*	0.0188 ± 0.6	0.1113 ± 6.1	23.238 ± 6.1	0.09	119.8 ± 0.7	107.1 ± 6.2	− 166 ± 76	120.6 ± 0.8
28-4c	39	*NA*	0.0186 ± 0.8	0.1282 ± 4.5	19.962 ± 4.4	0.17	118.6 ± 0.9	122.5 ± 5.2	199 ± 51	118.3 ± 1.0
28-5c	61	*NA*	0.0193 ± 1.1	0.1293 ± 3.9	20.555 ± 3.7	0.29	123.1 ± 1.3	123.4 ± 4.5	131 ± 43	123.0 ± 1.4
28-6c	65	*NA*	0.0180 ± 0.7	0.1324 ± 5.0	18.723 ± 5.0	0.14	114.9 ± 0.8	126.3 ± 5.9	346 ± 56	114.2 ± 0.9
28-7c	88	*NA*	0.0194 ± 0.5	0.1615 ± 1.6	16.558 ± 1.5	0.30	123.8 ± 0.6	152.0 ± 2.2	618 ± 16	122.0 ± 0.6
28-8c	99	*NA*	0.0190 ± 0.4	0.1491 ± 1.6	17.582 ± 1.5	0.26	121.4 ± 0.5	141.1 ± 2.1	487 ± 17	120.1 ± 0.5
28-9c	134	*NA*	0.0188 ± 0.4	0.1415 ± 1.4	18.321 ± 1.3	0.31	120.1 ± 0.5	134.4 ± 1.8	395 ± 15	119.1 ± 0.5
28-10c	141	*NA*	0.0184 ± 0.6	0.1387 ± 1.3	18.293 ± 1.2	0.44	117.6 ± 0.7	131.9 ± 1.6	399 ± 13	116.7 ± 0.7
28-11c	207	*NA*	0.0180 ± 0.7	0.1252 ± 1.6	19.831 ± 1.4	0.44	115.1 ± 0.8	119.8 ± 1.8	215 ± 16	114.8 ± 0.8
28-12c	127	*NA*	0.0191 ± 0.4	0.1546 ± 1.7	17.014 ± 1.6	0.26	121.9 ± 0.5	146.0 ± 2.3	559 ± 18	120.3 ± 0.5
28-13c	144	*NA*	0.0188 ± 0.4	0.1343 ± 1.6	19.262 ± 1.6	0.25	119.8 ± 0.5	127.9 ± 1.9	282 ± 18	119.3 ± 0.5
28-14c	*77*	*NA*	*0.0209 ± 1.2*	*0.1565 ± 3.0*	*18.402 ± 2.8*	*0.40*	*133.2 ± 1.6*	*147.6 ± 4.1*	*385 ± 31*	*132.3 ± 1.6*
28-15c	155	*NA*	0.0180 ± 0.4	0.1224 ± 2.4	20.320 ± 2.4	0.17	115.3 ± 0.5	117.3 ± 2.7	158 ± 28	115.2 ± 0.5
28-16c	47	*NA*	0.0176 ± 1.2	0.0924 ± 6.0	26.258 ± 5.9	0.21	112.4 ± 1.4	89.7 ± 5.1	− 479 ± 77	113.8 ± 1.4
28-17c	80	*NA*	0.0182 ± 0.7	0.1121 ± 3.4	22.338 ± 3.4	0.20	116.0 ± 0.8	107.9 ± 3.5	− 68 ± 41	116.5 ± 0.8
28-18c	57	*NA*	0.0192 ± 0.9	0.1467 ± 3.6	18.025 ± 3.5	0.25	122.4 ± 1.1	139.0 ± 4.7	432 ± 39	121.4 ± 1.1
28-19c	24	*NA*	0.0185 ± 0.6	0.1087 ± 2.0	23.464 ± 1.9	0.32	118.1 ± 0.7	104.8 ± 2.0	− 190 ± 24	119.0 ± 0.8
28-20c	40	*NA*	0.0186 ± 0.5	0.1159 ± 7.5	22.120 ± 7.4	0.07	118.8 ± 0.6	111.4 ± 7.8	− 44 ± 90	119.3 ± 0.8
28-21c	36	*NA*	0.0187 ± 0.5	0.1155 ± 8.1	22.364 ± 8.1	0.06	119.7 ± 0.6	111.0 ± 8.5	− 71 ± 98	120.2 ± 0.8
28-22c	68	*NA*	0.0184 ± 0.4	0.1414 ± 3.8	17.914 ± 3.8	0.11	117.3 ± 0.5	134.2 ± 4.7	445 ± 42	116.2 ± 0.6
5a1c	24	*NA*	0.0190 ± 1.1	0.0940 ± 13.8	27.826 ± 13.7	0.08	121.2 ± 1.3	91.2 ± 12.0	− 636 ± 188	123.1 ± 1.5
5a2c	24	*NA*	0.0185 ± 1.0	0.1592 ± 6.9	16.040 ± 6.8	0.15	118.3 ± 1.2	150.0 ± 9.5	686 ± 73	116.2 ± 1.3
5a3c	*23*	*NA*	*0.0248 ± 0.5*	*0.1744 ± 14.4*	*19.614 ± 14.4*	*0.03*	*158.0 ± 0.7*	*163.3 ± 21.5*	*240 ± 166*	*157.7* ± 1.6
5a4c	31	*NA*	0.0187 ± 0.8	0.1084 ± 7.6	23.806 ± 7.6	0.11	119.5 ± 1.0	104.5 ± 7.5	− 226 ± 95	120.5 ± 1.1
5a5c	27	*NA*	0.0180 ± 0.9	0.0856 ± 17.8	28.890 ± 17.8	0.05	114.7 ± 1.1	83.4 ± 14.2	− 740 ± 249	116.6 ± 1.4
5a6c	27	*NA*	0.0176 ± 1.0	0.0858 ± 11.4	28.296 ± 11.3	0.08	112.5 ± 1.1	83.6 ± 9.1	− 682 ± 156	114.4 ± 1.2
5a7c	28	*NA*	0.0179 ± 0.6	0.1245 ± 7.9	19.820 ± 7.9	0.08	114.3 ± 0.7	119.1 ± 8.9	216 ± 92	114.0 ± 0.9
5a8c	31	*NA*	0.0174 ± 1.0	0.1216 ± 6.8	19.771 ± 6.7	0.14	111.4 ± 1.1	116.5 ± 7.4	222 ± 77	111.1 ± 1.2
5a9c	39	*NA*	0.0178 ± 1.0	0.1153 ± 7.3	21.276 ± 7.2	0.14	113.7 ± 1.1	110.8 ± 7.6	49 ± 86	113.9 ± 1.2
5a10c	27	*NA*	0.0182 ± 0.9	0.1258 ± 10.7	19.889 ± 10.6	0.09	115.9 ± 1.0	120.3 ± 12.0	208 ± 123	115.7 ± 1.3
5a11c	35	*NA*	0.0180 ± 0.5	0.0627 ± 13.6	39.460 ± 13.6	0.03	114.7 ± 0.5	61.8 ± 8.1	− 1711 ± 237	118.0 ± 0.7
5a12c	39	*NA*	0.0181 ± 0.6	0.0992 ± 12.9	25.174 ± 12.9	0.04	115.7 ± 0.7	96.0 ± 11.8	− 369 ± 168	116.9 ± 1.0
5a13c	22	*NA*	0.0180 ± 0.8	0.0975 ± 9.5	25.394 ± 9.4	0.08	114.8 ± 0.9	94.5 ± 8.5	− 391 ± 123	116.0 ± 1.1
5a14c	48	*NA*	0.0178 ± 0.8	0.1025 ± 5.4	23.944 ± 5.4	0.15	113.8 ± 0.9	99.1 ± 5.1	− 241 ± 68	114.7 ± 1.0
5a15c	24	*NA*	0.0186 ± 0.8	0.1403 ± 6.8	18.239 ± 6.8	0.11	118.5 ± 0.9	133.3 ± 8.5	405 ± 76	117.6 ± 1.0
5a16c	42	*NA*	0.0176 ± 0.9	0.0996 ± 6.6	24.380 ± 6.6	0.13	112.6 ± 1.0	96.4 ± 6.1	− 287 ± 84	113.6 ± 1.0
5a17c	20	*NA*	0.0186 ± 0.9	0.1028 ± 12.1	24.929 ± 12.0	0.07	118.7 ± 1.0	99.4 ± 11.4	− 344 ± 155	120.0 ± 1.3
5a18c	32	*NA*	0.0185 ± 0.9	0.1570 ± 9.4	16.198 ± 9.4	0.09	117.8 ± 1.0	148.1 ± 12.9	665 ± 101	115.9 ± 1.3
5a19c	36	*NA*	0.0194 ± 1.1	0.1317 ± 9.3	20.285 ± 9.2	0.11	123.8 ± 1.3	125.7 ± 10.9	162 ± 108	123.6 ± 1.5
5a20c	25	*NA*	0.0188 ± 0.9	0.1471 ± 8.4	17.584 ± 8.4	0.11	119.8 ± 1.1	139.3 ± 10.9	486 ± 92	118.5 ± 1.3
221K-1t	267	18051	0.0206 ± 0.7	0.1309 ± 2.8	21.669 ± 2.7	0.25	131.3 ± 0.9	124.9 ± 3.7	5 ± 33	NA
221K-2t	351	29570	0.0200 ± 0.5	0.1267 ± 1.9	21.757 ± 1.8	0.26	127.6 ± 0.6	121.2 ± 2.4	− 4 ± 22	NA

Table 2 (*continued*)

Sample	U (ppm)	$^{206}Pb/^{204}Pb$ ratio	$^{206}Pb/^{238}U \pm$ ratio (%)	$^{207}Pb/^{235}U \pm$ ratio (%)	$^{206}Pb/^{207}P \pm$ ratio (%)	Error correction	$^{206}Pb/^{238}U \pm$ age (Ma)	$^{207}Pb/^{235}U \pm$ age (Ma)	$^{206}Pb/^{207}Pb \pm$ age (Ma)	^{207}Pb correction $\pm$ age (Ma)
221K-3t	428	36509	0.0198 ± 0.6	0.1297 ± 1.6	21.040 ± 1.4	0.41	126.3 ± 0.8	123.8 ± 2.0	76 ± 17	NA
221K-4c	*262*	*43226*	*0.0364 ± 1.4*	*0.2498 ± 1.9*	*20.096 ± 1.4*	*0.71*	*230.5 ± 3.2*	*226.4 ± 4.9*	*184 ± 16*	*NA*
221K-5c	40	4497	0.0577 ± 0.9	0.4339 ± 4.0	18.347 ± 3.9	0.23	361.8 ± 3.3	365.9 ± 17.3	392 ± 43	NA
221K-6c	44	15551	0.0560 ± 1.0	0.4324 ± 4.7	17.856 ± 4.6	0.22	351.2 ± 3.7	364.8 ± 20.4	453 ± 51	NA
221K-7c	15	7790	0.0569 ± 1.2	0.3726 ± 16.6	21.039 ± 16.6	0.07	356.4 ± 4.4	321.6 ± 60.9	76 ± 197	NA
221K-8c	90	38799	0.0580 ± 0.8	0.4120 ± 3.5	19.416 ± 3.4	0.23	363.6 ± 3.0	350.3 ± 14.5	263 ± 39	NA
221K-9t	118	12730	0.0202 ± 1.5	0.1271 ± 6.8	21.893 ± 6.6	0.23	128.8 ± 2.0	121.5 ± 8.7	− 19 ± 80	NA
221K-10t	*56*	*6095*	*0.0261 ± 1.3*	*0.2049 ± 9.5*	*17.538 ± 9.5*	*0.14*	*165.9 ± 2.2*	*189.3 ± 19.6*	*492 ± 104*	*NA*
221K-11c	*94*	*18096*	*0.0502 ± 1.2*	*0.3895 ± 7.1*	*17.782 ± 7.0*	*0.17*	*315.9 ± 3.9*	*334.0 ± 27.7*	*462 ± 77*	*NA*
221K-12c	101	16611	0.0570 ± 1.0	0.4402 ± 2.0	17.864 ± 1.8	0.49	357.5 ± 3.6	370.4 ± 9.0	452 ± 19	NA
221K-13c	99	26804	0.0583 ± 1.0	0.4178 ± 3.1	19.225 ± 3.0	0.32	365.0 ± 3.8	354.5 ± 13.1	286 ± 34	NA
221K-14c	74	22844	0.0575 ± 1.1	0.4156 ± 2.2	19.089 ± 1.9	0.51	360.6 ± 4.2	352.9 ± 9.3	302 ± 22	NA
221K-15t	67	11424	0.0205 ± 1.8	0.1253 ± 11.0	22.504 ± 10.8	0.16	130.5 ± 2.4	119.8 ± 13.9	− 86 ± 133	NA
221K-16c	*152*	*29614*	*0.0513 ± 2.9*	*0.3736 ± 4.9*	*18.927 ± 4.0*	*0.58*	*322.4 ± 9.4*	*322.3 ± 18.4*	*322 ± 45*	*NA*
221K-17c	*95*	*23260*	*0.0496 ± 1.1*	*0.3565 ± 3.6*	*19.191 ± 3.4*	*0.31*	*312.2 ± 3.5*	*309.6 ± 12.8*	*290 ± 39*	*NA*
221K-18c	*100*	*18092*	*0.0535 ± 3.2*	*0.3782 ± 7.7*	*19.504 ± 7.0*	*0.42*	*336.0 ± 11.1*	*325.7 ± 29.1*	*253 ± 80*	*NA*
221K-19c	491	23329	0.0574 ± 0.9	0.4329 ± 2.3	18.274 ± 2.1	0.40	360.1 ± 3.4	365.8 ± 10.3	401 ± 24.0	NA
221K-20c	196	9298	0.0567 ± 0.6	0.4178 ± 2.6	18.723 ± 2.5	0.22	356.3 ± 2.0	354.9 ± 11.7	346 ± 28.0	NA
221K-21c	*121*	*4240*	*0.0422 ± 0.6*	*0.2875 ± 3.1*	*20.220 ± 3.0*	*0.19*	*266.2 ± 1.5*	*257.2 ± 9.2*	*169 ± 35.0*	*NA*
221K-22c	827	8487	0.0190 ± 3.0	0.1263 ± 3.7	20.737 ± 2.1	0.82	121.8 ± 3.7	121.4 ± 5.2	110 ± 25.0	NA
221K-23t	964	8645	0.0206 ± 0.3	0.1402 ± 2.1	20.257 ± 2.1	0.16	131.5 ± 0.4	133.7 ± 3.6	165 ± 24.0	NA
221K-24c	*370*	*19432*	*0.0501 ± 1.0*	*0.3744 ± 2.5*	*18.451 ± 2.3*	*0.40*	*315.3 ± 3.1*	*323.2 ± 2.7*	*379 ± 25.0*	*NA*
221K-25c	548	33147	0.0594 ± 0.9	0.4508 ± 2.2	18.153 ± 2.0	0.41	372.1 ± 3.5	378.3 ± 10.3	416 ± 23.0	NA
221K-26c	*882*	*4216*	*0.0862 ± 1.7*	*3.1545 ± 4.6*	*3.770 ± 4.2*	*0.38*	*533.8 ± 9.6*	*1446.0 ± 136.8*	*3278 ± 33.0*	*NA*
221K-27t	166	1708	0.0591 ± 0.9	0.6847 ± 5.1	11.890 ± 5.0	0.18	370.0 ± 3.6	530.6 ± 35.1	1295 ± 49.0	NA
221K-28t	*480*	*22242*	*0.0448 ± 1.6*	*0.3304 ± 2.6*	*18.677 ± 2.1*	*0.59*	*282.2 ± 4.5*	*290.1 ± 9.1*	*352 ± 24.0*	*NA*
221K-29c	*1150*	*30148*	*0.0480 ± 2.2*	*0.3685 ± 3.0*	*17.952 ± 2.0*	*0.74*	*302.2 ± 6.8*	*319.8 ± 11.9*	*441 ± 22.0*	*NA*
221K-30c	829	29551	0.0594 ± 0.5	0.4506 ± 2.1	18.183 ± 2.0	0.22	372.4 ± 1.8	378.4 ± 9.0	412 ± 22.0	NA
221K-31c	108	7676	0.0589 ± 0.9	0.4254 ± 2.6	19.100 ± 2.5	0.33	369.0 ± 3.3	360.5 ± 11.1	301 ± 28.0	NA
221K-32c	179	10102	0.0580 ± 0.4	0.4291 ± 2.4	18.619 ± 2.4	0.16	363.5 ± 1.4	363.1 ± 10.7	359 ± 27.0	NA
221K-33c	819	33551	0.0596 ± 0.8	0.4537 ± 2.2	18.100 ± 2.0	0.35	373.1 ± 2.9	380.8 ± 10.4	422 ± 23.0	NA
221K-34t	143	13634	0.0184 ± 4.5	0.1306 ± 11.9	19.389 ± 11.0	0.38	117.7 ± 5.3	125.9 ± 16.3	267 ± 126.0	NA
221K-35t	68	2536	0.0560 ± 0.5	0.4308 ± 4.6	17.934 ± 4.6	0.10	351.8 ± 1.7	364.2 ± 20.2	443 ± 51.0	NA
221K-36c	136	4135	0.0574 ± 0.7	0.4827 ± 2.8	16.388 ± 2.7	0.24	360.2 ± 2.5	400.0 ± 14.8	640 ± 29.0	NA
221K-37t	278	24793	0.0561 ± 0.7	0.4215 ± 2.3	18.361 ± 2.2	0.32	352.4 ± 2.6	357.4 ± 10.1	390 ± 24.0	NA
221K-38t	*234*	*8850*	*0.0233 ± 0.9*	*0.1544 ± 3.6*	*20.767 ± 3.5*	*0.25*	*148.9 ± 1.3*	*146.6 ± 6.2*	*107 ± 41.0*	*NA*
221K-39c	265	22663	0.0606 ± 0.3	0.4561 ± 2.2	18.310 ± 2.1	0.16	379.0 ± 1.3	382.3 ± 10.7	396 ± 24.0	NA
221K-40t	*155*	*4240*	*0.0537 ± 1.1*	*0.3853 ± 3.0*	*19.218 ± 2.8*	*0.36*	*337.3 ± 3.8*	*331.7 ± 12.6*	*287 ± 32.0*	*NA*
221K-41t	51	16902	0.0586 ± 1.1	0.4362 ± 3.7	18.535 ± 3.6	0.30	367.1 ± 4.2	368.1 ± 16.6	369 ± 40.0	NA
221K-42t	49	4837	0.0584 ± 1.1	0.4686 ± 5.4	17.185 ± 5.3	0.21	366.0 ± 4.2	0.3 ± 26.3	537 ± 58.0	NA
221K-43t	42	2299	0.0595 ± 1.1	0.4142 ± 5.2	19.809 ± 5.1	0.21	373.3 ± 4.3	352.7 ± 22.0	217 ± 59.0	NA
221K-44t	192	6125	0.0203 ± 2.3	0.1206 ± 4.0	23.251 ± 3.3	0.57	130.6 ± 3.0	116.5 ± 5.5	− 167 ± 41.0	NA
221K-45t	187	45340	0.0576 ± 0.5	0.4275 ± 2.3	18.578 ± 2.3	0.23	361.3 ± 2.0	361.0 ± 10.1	364 ± 26.0	NA
221K-46t	35	4453	0.0588 ± 1.7	0.4522 ± 8.9	17.926 ± 8.8	0.19	368.5 ± 6.3	379.2 ± 40.3	444 ± 98.0	NA
221K-47c	59	10614	0.0573 ± 0.9	0.4391 ± 4.5	17.975 ± 4.5	0.20	359.1 ± 3.0	370.5 ± 20.6	438 ± 49.0	NA

(*continued on next page*)

Table 2 (*continued*)

Sample	U (ppm)	$^{206}Pb/^{204}Pb$ ratio	$^{206}Pb/^{238}U \pm$ ratio (%)	$^{207}Pb/^{235}U \pm$ ratio (%)	$^{206}Pb/^{207}P \pm$ ratio (%)	Error correction	$^{206}Pb/^{238}U \pm$ age (Ma)	$^{207}Pb/^{235}U \pm$ age (Ma)	$^{206}Pb/^{207}Pb \pm$ age (Ma)	^{207}Pb correction $\pm$ age (Ma)
221K-48c	67	9742	0.0580 ± 1.0	0.4275 ± 4.6	18.699 ± 4.4	0.23	363.8 ± 4.0	361.1 ± 20.4	349 ± 50.0	NA
221K-49c	90	18019	0.0591 ± 1.0	0.4423 ± 4.0	18.413 ± 3.9	0.25	370.4 ± 4.0	372.8 ± 18.9	384 ± 44.0	NA
221K-50c	26	2991	0.0601 ± 1.1	0.4130 ± 4.4	20.052 ± 4.3	0.24	376.4 ± 4.0	351.1 ± 18.0	189 ± 50.0	NA
ADA2-1c	314	16959	0.0323 ± 0.9	0.2236 ± 1.6	19.907 ± 1.3	0.54	204.8 ± 1.8	204.9 ± 3.6	206 ± 15	NA
ADA2-2c	729	3605	0.0319 ± 0.5	0.2051 ± 1.0	21.437 ± 0.9	0.49	202.3 ± 1.0	189.4 ± 2.0	31 ± 10	NA
ADA2-3c	125	6567	0.0315 ± 1.0	0.2113 ± 4.2	20.563 ± 4.0	0.25	200.0 ± 2.1	194.6 ± 8.9	130 ± 47	NA
ADA2-4c	128	4641	0.0320 ± 0.4	0.1987 ± 3.2	22.200 ± 3.2	0.12	203.0 ± 0.8	184.0 ± 6.5	− 53 ± 39	NA
ADA2-5c	*53*	*17623*	*0.0302 ± 0.6*	*0.1870 ± 7.4*	*22.282 ± 7.4*	*0.07*	*191.9 ± 1.1*	*174.0 ± 14.0*	*− 62 ± 90*	*NA*
ADA2-6c	70	2532	0.0319 ± 0.6	0.2188 ± 4.8	20.080 ± 4.7	0.13	202.2 ± 1.3	200.9 ± 10.6	186 ± 55	NA
ADA2-7c	30	15567	0.0323 ± 1.5	0.2033 ± 16.4	21.890 ± 16.3	0.09	204.8 ± 3.1	187.9 ± 33.3	− 19 ± 197	NA
ADA2-8c	81	2624	0.0318 ± 0.6	0.1967 ± 5.6	22.305 ± 5.6	0.11	201.9 ± 1.3	182.3 ± 11.1	− 65 ± 68	NA
ADA2-9c	135	212500	0.0316 ± 2.0	0.2363 ± 3.8	18.429 ± 3.2	0.53	200.4 ± 4.1	215.4 ± 9.0	382 ± 36	NA
ADA2-10c	59	176999	0.0317 ± 0.9	0.2102 ± 12.0	20.796 ± 11.9	0.08	201.2 ± 1.9	193.7 ± 25.2	103 ± 141	NA
ADA2-11c	*54*	*6500*	*0.0271 ± 1.1*	*0.1906 ± 11.4*	*19.602 ± 11.3*	*0.10*	*172.3 ± 2.0*	*177.1 ± 21.8*	*242 ± 131*	*NA*
ADA2-12c	94	3222	0.0322 ± 0.5	0.2014 ± 6.7	22.062 ± 6.7	0.07	204.4 ± 1.0	186.3 ± 13.7	− 38 ± 82	NA
ADA2-13c	*48*	*1570*	*0.0258 ± 0.7*	*0.1465 ± 14.3*	*24.243 ± 14.3*	*0.05*	*164.0 ± 1.1*	*138.8 ± 21.0*	*− 272 ± 181*	*NA*
ADA2-14c	*43*	*13125*	*0.0236 ± 1.4*	*0.1503 ± 18.9*	*21.688 ± 18.9*	*0.07*	*150.6 ± 2.1*	*142.2 ± 28.4*	*3 ± 227*	*NA*
ADA2-15c	162	32272	0.0325 ± 1.0	0.2277 ± 2.9	19.675 ± 2.7	0.34	206.2 ± 2.0	208.3 ± 6.6	233 ± 31	NA
ADA2-16c	132	12743	0.0327 ± 0.6	0.2176 ± 3.7	20.728 ± 3.6	0.16	207.5 ± 1.2	199.9 ± 8.1	111 ± 43	NA
ADA2-17c	90	18709	0.0328 ± 0.5	0.2286 ± 5.4	19.775 ± 5.4	0.09	208.0 ± 1.1	209.0 ± 12.5	221 ± 62	NA
ADA2-18c	125	3783	0.0322 ± 0.8	0.2325 ± 3.9	19.085 ± 3.8	0.20	204.2 ± 1.6	212.2 ± 9.1	303 ± 43	NA
ADA2-19c	63	3726	0.0325 ± 1.1	0.2299 ± 6.5	19.478 ± 6.4	0.18	206.0 ± 2.4	210.1 ± 14.9	256 ± 73	NA
ADA2-20c	*38*	*13947*	*0.0279 ± 1.1*	*0.1673 ± 13.1*	*22.960 ± 13.1*	*0.08*	*177.1 ± 2.0*	*157.0 ± 22.1*	*− 136 ± 162*	*NA*
ADA2-21c	*44*	*8748*	*0.0240 ± 0.7*	*0.1499 ± 12.3*	*22.026 ± 12.3*	*0.06*	*152.6 ± 1.1*	*141.9 ± 18.5*	*− 34 ± 149*	*NA*
ADA2-22c	99	26510	0.0332 ± 0.6	0.2388 ± 4.4	19.175 ± 4.4	0.14	210.6 ± 1.3	217.5 ± 10.7	292 ± 50	NA
ADA2-23c	162	37708	0.0316 ± 0.6	0.2342 ± 2.6	18.621 ± 2.6	0.23	200.8 ± 1.2	213.7 ± 6.3	359 ± 29	NA
ADA2-24c	330	48018	0.0329 ± 0.8	0.2430 ± 1.6	18.657 ± 1.4	0.48	208.5 ± 1.6	220.8 ± 4.0	354 ± 16	NA
ADA2-25c	39	7083	0.0328 ± 1.7	0.2370 ± 12.2	19.084 ± 12.1	0.14	208.1 ± 3.5	216.0 ± 28.9	303 ± 137	NA
ADA2-26t	145	2506	0.0177 ± 6.2	0.1220 ± 9.3	19.989 ± 7.0	0.66	113.0 ± 7.0	116.8 ± 11.5	196 ± 82	NA
ADA2-27t	*43*	*1987*	*0.0252 ± 1.3*	*0.1605 ± 14.2*	*21.628 ± 14.1*	*0.09*	*160.2 ± 2.0*	*151.1 ± 22.8*	*10 ± 170*	*NA*
ADA2-28t	44	5893	0.0187 ± 1.0	0.1249 ± 4.4	20.597 ± 4.3	0.22	119.1 ± 1.2	119.5 ± 5.6	126 ± 51	NA
ADA2-29t	*107*	*4837*	*0.0196 ± 0.5*	*0.1382 ± 1.1*	*19.529 ± 1.0*	*0.42*	*124.9 ± 0.6*	*131.4 ± 1.6*	*250 ± 12*	*NA*
ADA2-30t	77	1348	0.0180 ± 1.1	0.1040 ± 2.3	23.825 ± 2.1	0.45	114.8 ± 1.2	100.4 ± 2.5	− 228 ± 26	NA
ADA2-31t	75	20322	0.0175 ± 1.1	0.1416 ± 6.4	17.042 ± 6.3	0.17	111.8 ± 1.2	134.4 ± 9.1	555 ± 69	NA
ADA2-32t	205	1111	0.0175 ± 0.9	0.0982 ± 1.9	24.544 ± 1.6	0.49	111.7 ± 1.0	95.1 ± 1.9	− 304 ± 21	NA
ADA2-33t	107	1503	0.0190 ± 1.3	0.1139 ± 1.7	23.000 ± 1.2	0.74	121.4 ± 1.6	109.6 ± 2.0	− 140 ± 14	NA
ADA2-34t	*20*	*33533*	*0.0196 ± 0.7*	*0.1456 ± 2.2*	*18.590 ± 2.1*	*0.32*	*125.3 ± 0.9*	*138.0 ± 3.2*	*362 ± 23*	*NA*
ADA2-35t	79	7649	0.0187 ± 4.9	0.1440 ± 13.3	17.874 ± 12.3	0.37	119.2 ± 5.9	136.6 ± 19.2	450 ± 137	NA
ADA2-36t	363	4293	0.0181 ± 1.2	0.1192 ± 6.7	20.934 ± 6.6	0.18	115.6 ± 1.4	114.3 ± 8.1	88 ± 78	NA
ADA2-37t	27	1387	0.0188 ± 2.4	0.1489 ± 6.6	17.411 ± 6.1	0.37	120.1 ± 2.9	140.9 ± 9.9	508 ± 67	NA
ADA2-38t	20	1362	0.0183 ± 3.7	0.1107 ± 7.1	22.817 ± 6.0	0.53	117.0 ± 4.4	106.6 ± 7.9	− 120 ± 74	NA
ADA2-39t	37	3061	0.0182 ± 2.0	0.1087 ± 6.3	23.083 ± 6.0	0.32	116.3 ± 2.4	104.8 ± 7.0	− 149 ± 74	NA
ADA2-40t	143	18329	0.0180 ± 3.7	0.1280 ± 11.8	19.412 ± 11.2	0.31	115.2 ± 4.3	122.3 ± 15.2	264 ± 129	NA
ADA2-41t	644	15254	0.0184 ± 0.9	0.0870 ± 3.6	29.202 ± 3.5	0.24	117.7 ± 1.0	84.7 ± 3.2	− 770 ± 49	NA
ADA2-42t	30	5509	0.0189 ± 0.8	0.1384 ± 1.6	18.837 ± 1.4	0.50	120.8 ± 1.0	131.6 ± 2.3	333 ± 16	NA

Table 2 (*continued*)

Sample	U (ppm)	$^{206}Pb/^{204}Pb$ ratio	$^{206}Pb/^{238}U$ ± ratio (%)	$^{207}Pb/^{235}U$ ± ratio (%)	$^{206}Pb/^{207}P$ ± ratio (%)	Error correction	$^{206}Pb/^{238}U$ ± age (Ma)	$^{207}Pb/^{235}U$ ± age (Ma)	$^{206}Pb/^{207}Pb$ ± age (Ma)	^{207}Pb correction ± age (Ma)
ADA2-43t	292	47142	0.0178 ± 0.7	0.1255 ± 2.3	19.518 ± 2.2	0.31	113.5 ± 0.8	120.1 ± 2.9	251 ± 25	NA
ADA2-44t	221	10947	0.0180 ± 1.6	0.1198 ± 5.1	20.733 ± 4.9	0.30	115.1 ± 1.8	114.9 ± 6.2	111 ± 58	NA
ADA2-45t	52	6595	0.0180 ± 1.2	0.1309 ± 2.8	18.951 ± 2.5	0.42	115.0 ± 1.3	124.9 ± 3.7	319 ± 28	NA

Analyses in italics are not used in age calculations. Position of spot: c = core, t = tip. NA = information not available. U concentration has an uncertainty of ~25%. $^{206}Pb/^{238}U$ and $^{206}Pb/^{207}Pb$ ratios have been corrected for fractionation using a factor determined from analysis of a zircon crystal of known age. Uncertainties are shown at 1σ level. ^{207}Pb correction age is determined by adjusting the common Pb correction to make radiogenic $^{206}Pb/^{238}U$ and $^{206}Pb/^{207}Pb$ ages concordant. For samples 9935, 221K, and ADA2, common Pb correction is from measured $^{206}Pb/^{204}Pb$.

Daniel. In addition, the steep upper amphibolite facies foliations (S_{SZ}) of the Indecision Creek Shear Zone cut across the lower (and eastern) contact of the WFO east of Mt. Daniel (Figs. 9b and 10d). These relationships indicate that once the WFO crystallized deformation was no longer concentrated in a narrow melt-enhanced zone at the base of the batholith. By ~116 Ma (and possibly earlier) this zone had been replaced by the steep shear zones up to 15 km wide. This represents a progressive widening of the zone of deformation below the batholith to include the entire lower crustal section between Milford and Caswell Sounds.

Following dehydration of the lower crust and abandonment of the Mt. Daniel Shear Zone physical and kinematic links developed above and below the WFO. The Caswell fold–thrust belt continued to evolve in the middle crust following crystallization of the batholith and records arc-normal contraction and vertical thickening with a sinistral component of arc-parallel displacement. The George Sound and Indecision Creek Shear Zones also record subhorizontal arc-normal contraction and vertical (layer-perpendicular) thickening with components of sinistral arc-parallel displacement. The simultaneous or near simultaneous development of these contractional structures confirms indicate that the middle and lower crust were coupled kinematically above and below the batholith.

The style of contractional deformation affecting the upper crust prior to ~105 Ma resembles the style of deformation in the Caswell Thrust Belt (Fig. 9b). Narrow thrust zones and steeply dipping foliations with down-dip lineations were localized within the contact aureoles of plutons on the western side of the Median Batholith in Westland and on the eastern side east of Fiordland (Bradshaw, 1989a; Tulloch and Challis, 2000). On Stewart Island, dipping thrust faults formed inside the batholith during ~125–105 Ma magmatism (Allibone and Tulloch, 1997; Tulloch and Kimbrough, 2003). These structural patterns where deformation was concentrated in a narrow (50–75 km wide) zone inside and on both sides of the Median Batholith are remarkably similar to those preserved in Fiordland where thrusts deform both pluton and country rock in the contact aureoles of the WFO (Figs. 9a and 10d). These relationships provide evidence that the upper, middle and lower crusts were coupled kinematically during ~116–105 Ma contraction as plutons were emplaced into the upper crust.

9. Discussion: controls on vertical coupling and decoupling in the crust

9.1. Changing strength and rheology of the lower crust

Structural and metamorphic relationships within northern Fiordland suggest that decoupling of the middle and lower crust above and below the WFO occurred as large volumes of magma (>10 km thickness) were emplaced into

and moved through a lower crust weakened by melt and heat. Two of the dominant processes controlling decoupling during this period were the rates of emplacement and crystallization of the WFO and the duration of the thermal pulse that accompanied the magmatism. Rapid rates of emplacement and cooling are implied by available geochronologic and metamorphic data (Fig. 10a). Crystallization ages (Tulloch and Kimbrough, 2003; Hollis et al., 2004) suggest that most of the WFO was emplaced into the lower crust within the period ~126–120 Ma. By ~120 Ma, garnet granulite facies metamorphism at temperatures of 750 °C < T < 850 °C affected large regions of the batholith and its lower crustal host (Clarke et al., 2000; Tulloch et al., 2000; Hollis et al., 2003). By ~116 Ma kyanite- and paragonite-bearing assemblages replaced the older garnet-, clinopyroxene-bearing granulite facies assemblages indicating that the lower crust below the batholith had cooled to temperatures of T = 650–700 °C (Daczko et al., 2002c). The age of ~116 Ma is an average of the metamorphic rims dates obtained from the Caswell Sound fold–thrust belt and the Indecision Creek Shear Zone (samples 995a and Ada2, Fig. 8).

Simple one-dimensional models of conductive heat loss using standard solutions to the heat flow equation (Spear, 1993, p. 43) support the interpretation of rapid cooling of the WFO by ~116 Ma. Magma compositions and the liquidus temperature of basalt suggest that initial intrusions temperatures were close to T = 1200 °C following the estimates of Petford and Gallagher (2001). Advective removal of heat via fluid and melt transfer and the thrusting of pre-existing arc crust above and below the batholith during emplacement increases the rate of cooling. Burial and crustal thickening tend to slow the rate of cooling. However, metamorphic and geochronologic data from northern Fiordland indicate that most of the burial of the Arthur River Complex occurred prior to ~120 Ma granulite facies metamorphism (Fig. 10c). Calculations using metamorphic data to constrain ambient temperatures at ~120 Ma (T = 750–800 °C in crust below the batholith and T = 550–600 °C in crust above it) suggest that the thermal pulse accompanying WFO emplacement decayed to temperatures of T = 650–700 °C within ~3–4 million years. These results agree well with the mineral reactions that record cooling of the lower crust below the batholith (Daczko et al., 2002c). The well-known dependence of lower crustal strength and rheology on temperature, fluid activity and melt fraction imply that the lower crust experienced rapid changes in strength (effective viscosity) during the ~120–105 Ma period.

In addition to rates of cooling and magma emplacement, deformation patterns also were influenced by rheological contrasts and mechanical anisotropies created by the layered architecture of the lower crust. The influence of these features are revealed by the formation of shear zones in the contact aureoles of the batholith where steep temperature gradients and melt created strength contrasts and their parallelism with compositional layering (S_1) in host rock. The importance of inherited anisotropies has been observed in other orogens also (Klepeis and Crawford, 1999; Miller and Paterson, 2001).

Unlike the Mt. Daniel Shear Zone, the Caswell fold–thrust belt at the top of the WFO continued to develop as steep shear zones formed in the lowermost crust (Table 1). This heterogeneity appears to reflect differences in lithology at these two locations. As the WFO cooled, the strength contrast between the dioritic rock of the WFO and metasedimentary host rock at Caswell Sound continued to focus deformation. However, at Mt. Daniel similar bulk compositions between the WFO and its host rock meant that once the batholith had cooled to ambient temperatures, the contrast in strength across this zone was small. This interpretation explains differences in the thickness and duration of the shear zones. The relationships illustrate that crustal decoupling and the formation of subhorizontal or dipping shear zones in the deep crust strongly reflects local rheological contrasts and temperature gradients (see also Karlstrom and Williams, 2002).

The period of orogenesis characterized by high degrees of vertical coupling (Fig. 10d) coincided with the development of a strong, dry, mafic lower crustal root within northernmost Fiordland. A strengthening lower crust is implied in part by cooling. However, other processes also greatly influenced lower crustal strength. Piston cylinder experiments performed on unmelted samples of dioritic gneiss from the Pembroke Valley (Antignano, 2002) indicate that melt fractions remained low (≤10 vol%) at all temperatures up to T = 975 °C. Fluid absent melting of the gneiss was controlled by the decomposition of hornblende ± clinozoisite to produce garnet + melt and resulted in low melt volumes (Antignano, 2002; Klepeis et al., 2003). Klepeis et al. (2003) pointed out that although partial melting occurred in large parts of the lower crustal section (Fig. 10c), the total volumes of melt probably remained low. Low melt volumes would have helped the lower crust remain strong even as it partially melted. In addition, the formation of melt-induced fractures and vein networks by ~120 Ma aided melt extraction and escape from the lower crust (Daczko et al., 2001b). Klepeis and Clarke (2003) showed that ductile deformation in shear zones also aided melt escape. Davidson et al. (1994), Roering et al. (1995) and Rushmer (1995) report similar mechanisms of melt-enhanced embrittlement in the deep crust. These processes helped prevent the wholesale weakening of the lower crust following batholith emplacement.

In summary, the relationships we describe suggest that the development of a strong lower crustal root was aided by the following processes: (1) rapid cooling and crystallization of the WFO as pre-existing arc crust was thrust above and below the batholith; (2) the dehydration of the lower crust at granulite facies conditions; (3) the inherently high strength of mafic lower crustal rocks even as they underwent mineral reactions involving partial melting; (4)

low volumes of partial melt in the lower crust controlled by the decomposition of hornblende and clinozoisite; and (5) the rapid extraction of partial melt via a regionally extensive networks of fractures, veins and ductile shear zones.

The interplay among these processes illustrates the time-dependent nature of lower crustal rheology. This variability is consistent with data derived from rock deformation experiments that indicate melt volume, temperature, the mobilization of melt, and crustal composition cause variations in rock strength (Dell'Angelo and Tullis, 1988; Rushmer, 1995; Huerta et al., 1996; Rutter, 1997). The close relationships we observed among magmatism, elevated temperatures, melt-assisted strain localization, and vertical decoupling during the ~126–120 Ma period also are consistent with numerical and analytical models indicating that crust–mantle decoupling is characteristic of orogens with a weak lower crust. A weak, low viscosity zone in the lower crust causes stresses arising from mantle convergence preferentially to be transmitted horizontally rather than vertically through the crust (Royden, 1996; Ellis et al., 1998; Willett, 1998). The disparate strain paths we observed between different parts of the crustal section in Fiordland during WFO emplacement appear to reflect this process. Decoupling of the crust above and below the WFO is consistent with experimental data that show stress cannot be transmitted across zones containing more than ~30–45% volume melt (Rutter and Neumann, 1995).

The Fiordland example also illustrates spatially (both vertical and horizontal) variability of lower crustal strength profiles. The development of a relatively cool ($T = 650$–700 °C) lower crust in northernmost Fiordland by ~116 Ma contrasts with the elevated temperatures ($T > 800$ °C) at ~107.5 Ma recorded in granulite facies mineral assemblages ~100 km to the south in Doubtful Sound (Gibson and Ireland, 1995). Geochronologic and geochemical data also indicate that Na-rich magmas that reflect lower crustal sources continued to be emplaced into the middle and upper crust until ~105 Ma (Tulloch and Kimbrough, 2003). This magmatic activity at shallow crustal levels is compatible with data that suggest dikes and deformation ductile shear zones helped extract melt from the lower crust during the ~116–105 Ma period (Klepeis and Clarke, 2003; Klepeis et al., 2003). High degrees of vertical coupling thus occurred even as melt moved out of the lower crust and was emplaced into the upper crust until ~105 Ma. Together these observations imply that the effects of magmatism and partial melting on strength profiles and rheological transitions in the lower crust are much more transient and spatially heterogeneous than previously believed.

Finally, the features in the upper and lower crusts of the Fiordland–Westland orogen suggest that a highly viscous (strong, dry, mafic) lower crust influenced the overall structural style and partitioning of deformation vertically within the orogen. The narrow (50–75 km wide) focused style of contraction in the upper crust matches that predicted for orogens characterized by a highly viscous lower crust, where stresses derived from convergence and flow in the upper mantle preferentially are transmitted vertically through the crust (Royden, 1996; Ellis et al., 1998). In these types of orogens, the lower crust is not sufficiently weak to allow channelized lower crustal flow and crust–mantle decoupling during convergence.

9.2. Conditions influencing late-orogenic extension

The Fiordland–Westland orogen records the onset of extension (Fig. 10d) and the cessation of contraction by ~108–105 Ma (Tulloch and Kimbrough, 1989; Gibson and Ireland, 1995; Spell et al., 2000). This pattern invites comparison with other orogens that also exhibit evidence of late orogenic extension following a period of crustal thickening. The mechanisms that can contribute to this process are variable, including thermal relaxation of thickened lower crust (Vanderhaeghe and Teyssier, 1997, 2001), changes in convergence rate (England and Houseman, 1989), and the convective removal of a lithospheric root (Molnar et al., 1993). Below, we evaluate the possible roles of these mechanisms for the Fiordland–Westland orogen.

In vertically coupled orogens characterized by a highly viscous lower crust, contraction and extension can be balanced between different layers of the crust (e.g. Burg et al., 1984; Burchfield et al., 1992; Burg and Ford, 1997). Focused extension in the middle and upper crusts can occur simultaneously with shortening in the lower crust as a result of return flow away from the zone of mantle convergence (Royden, 1996). However, the timing of normal faulting in both the upper and lower crusts in the Fiordland–Westland eliminates this as a possible mechanism for this orogen. An alternative mechanism of late orogenic extension is a thermal weakening of previously thickened lower crust. In the Canadian Cordillera and the Himalaya–Tibet region, the onset of late orogenic extension has been linked to the thermal weakening of the middle or lower crust and an increased role of buoyancy forces due to partial melting (Royden, 1996; Vanderhaeghe and Teyssier, 1997; Ellis et al., 1998; Jamieson et al., 1998; Willett, 1998). This mechanism explains crosscutting relationships and differences in timing between contractional structures and normal faulting. However, we suggest that because we have evidence for a viscous, cooling, mafic lower crust and strong vertical coupling prior to the onset of extension (Fig. 10), we also can eliminate this as a possible mechanism of late orogenic extension. The relationships we observe in Fiordland suggest that late orogenic extension was caused by changes in horizontal forces derived from changing plate boundary dynamics (e.g. England and Houseman, 1989) rather than a changing lower crustal rheology or an increase in buoyancy forces arising from a thermal weakening of the lower crust during convergence.

10. Conclusions

A viscous, dry, mafic lower crust resulted in strong vertical coupling between the upper and lower crusts during Early Cretaceous contraction and orogenesis in western New Zealand. Vertical coupling lasted from ~116–105 Ma and may have begun by ~120 Ma. Transient vertical decoupling of the crust coincided with the emplacement of >10 km (thickness) of mafic–intermediate magma into the lower crust during the interval ~126–120 Ma. The development of a strong lower crustal root by ~116 Ma reflected the following conditions and processes: (1) cooling and crystallization of magma as pre-existing arc crust was thrust above and below the WFO batholith; (2) extensive dehydration of the lower crust at granulite facies conditions; (3) the inherently high strength of mafic lower crustal rocks as they underwent mineral reactions involving partial melting; (4) low volumes of partial melt in the lower crust controlled by the decomposition of hornblende ± clinozoisite in mafic crust; and (5) the rapid extraction of partial melt via melt-enhanced fracture networks, veins and ductile shear zones. Rheological contrasts and a viscous lower crust controlled the partitioning of deformation vertically within the orogen and produced a narrow (50–75 km wide), focused structural style in the upper crust. High degrees of vertical coupling occurred even as partial melts and magma moved out of the lower crust and were emplaced into the middle and upper crusts. The results imply that the onset of late orogenic extension at ~108–105 Ma was caused by a change in plate boundary dynamics rather than lateral flow of a weak lower crust during convergence. The Fiordland exposures provide an important natural example of the time-dependent, heterogeneous nature of lower crustal strength and rheology.

11. Uncited References

Karlstrom and Williams, 1995. Landis et al., 1999. Oliver, 1980. White and Jiang, 1994.

Acknowledgements

Funding to support this work was provided by National Science Foundation funding to KAK (EAR-0087323); Australian Research Council funding to KAK and GLC (ARC-A10009053); and funding from the Geological Society of America. We thank A. Tulloch for a helpful review; and N. Mortimer, I. Turnbull, T. Rushmer and W.C. Collins for discussions and assistance. We thank the Department of Land Conservation in Te Anau for permission to visit and sample localities in the Fiordland National Park. J. Hollis and T. Ireland provided assistance in compiling geochronologic data from northern Fiordland. J. Stevenson, A. Papadakis, A. Claypool, S. Marcotte and W.C. Simonson provided assistance in the field.

Appendix A. Analytical procedures for U–Pb isotopic analyses

Zircons were analyzed at the University of Arizona with a Micromass Isoprobe multicollector ICPMS equipped with 9 faraday collectors, an axial Daly detector, and 4 ion-counting channels. The Isoprobe is equipped with a DUV 193 laser ablation system from New Wave Research. The laser is a Compex 102 ArF Excimer laser, manufactured by Lamda Physik, with an emission wavelength of 193 nm. The analyses were conducted on 25–50 micron spots with an output energy of ~32 mJ and a repetition rate of 8 Hz. Each analysis consisted of one 30-s integration on the backgrounds (on peaks with no laser firing) and twenty 1-s integrations on peaks with the laser firing. The depth of each ablation pit is ~20 microns. The collector configuration allows simultaneous measurement of ^{204}Pb in a secondary electron multiplier while ^{206}Pb, ^{207}Pb, ^{208}Pb, ^{232}Th, and ^{238}U are measured with Faraday detectors. All analyses were conducted in static mode.

Correction for common Pb for most samples was performed by measuring ^{206}Pb/^{204}Pb, with the composition of common Pb from Stacey and Kramers (1975) and uncertainties of 1.0 for ^{206}Pb/^{204}Pb and 0.3 for ^{207}Pb/^{204}Pb. For two of the samples analyzed (995a and 9928), ^{204}Pb was not measured reliably, and common Pb was accounted for with a ^{207}Pb correction (Ludwig, 2001).

Fractionation of ^{206}Pb/^{238}U and ^{206}Pb/^{207}Pb during ablation was monitored by analyzing fragments of a large concordant zircon crystal that has a known (ID-TIMS) age of 564 ± 4 Ma (2σ; G.E. Gehrels, unpublished data). Typically this reference zircon was analyzed once for every four unknowns. The uncertainty arising from this calibration correction contributed ~2% systematic error to the ^{206}Pb/^{238}U and ^{206}Pb/^{207}Pb ages (2σ level). The uncertainty from decay constants and common Pb composition yielded an additional ~1% error to each analysis.

The reported ages are based primarily on ^{206}Pb/^{238}U ratios because the errors of the ^{207}Pb/^{235}U and ^{206}Pb/^{207}Pb ratios are significantly greater (Fig. 8; Table 2). This is due in large part to the low intensity (commonly ~1 mv) of the ^{207}Pb signal from these young grains. For each of the five samples (Fig. 8), the age data are plotted on a Pb/U concordia diagram, and the critical ^{206}Pb/^{238}U ages are shown on a separate age plot. The final age calculations are based on the weighted mean of the cluster of ^{206}Pb/^{238}U ages, with the error expressed both as the uncertainty of this mean and as the error of the age. The age error is based on the quadratic sum of the weighted mean error and the systematic error. Both are expressed at the 2σ level.

References

Allibone, A.H., Tulloch, A.J., 1997. Metasedimentary, granitoid and gabbroic rocks from central Stewart Island, New Zealand. New Zealand Journal of Geology and Geophysics 40, 53–68.

Antignano A., IV, 2002, Experimental constraints on granitoid compositions in convergent regimes: a geochemical study. M.Sc. Thesis, University of Vermont.

Axen, G.J., Selverstone, J., Byrne, T., Fletcher, J.M., 1998. If the strong crust leads, will the weak crust follow? GSA Today 8, 1–8.

Bishop, D.G., Bradshaw, J.D., Landis, C.A., 1985. Provisional terrain map of South Island, New Zealand. In: Howell, D.G., Jones, D.L., Cox, A., Nur, A. (Eds.), Tectonostratigraphic Terranes of the Circum–Pacific Region, Circum–Pacific Council for Energy and Resources, Houston, Texas, pp. 512–522.

Blattner, P., 1976. Replacement of hornblende by garnet in granulite facies assemblages near Milford Sound, New Zealand. Contributions to Mineralogy and Petrology 55, 181–190.

Blattner, P., 1991. The North Fiordland transcurrent convergence. New Zealand Journal of Geology and Geophysics 34, 543–553.

Blattner, P., Graham, I.G., 2000. New Zealand's Darran Complex and Mackay Intrusives—Rb/Sr whole-rock isochrons in the Median Tectonic Zone. American Journal of Science 300, 603–629.

Bradshaw, J.D., 1989. Cretaceous geotectonic patterns in the New Zealand region. Tectonics 8, 803–820.

Bradshaw, J.D., 1993. A review of the Median Tectonic Zone: terrane boundaries and terrane amalgamation near the Median Tectonic Line. New Zealand Journal of Geology and Geophysics 36, 117–125.

Bradshaw, J.Y., 1985. Geology of the northern Franklin Mountains, northern Fiordland, New Zealand, with emphasis on the origin and evolution of Fiordland granulites. Ph.D. thesis, University of Otago, New Zealand.

Bradshaw, J.Y., 1989a. Origin and metamorphic history of an Early Cretaceous polybaric granulite terrain, Fiordland, southwest New Zealand. Contribution to Mineralogy and Petrology 103, 346–360.

Bradshaw, J.Y., 1989b. Early Cretaceous vein-related garnet granulite in Fiordland, southwest New Zealand: a case for infiltration of mantle-derived CO_2-rich fluids. Journal of Geology 97, 697–717.

Bradshaw, J.Y., 1990. Geology of crystalline rocks of northern Fiordland: details of the granulite facies Western Fiordland Orthogneiss and associated rock units. New Zealand Journal of Geology and Geophysics 33, 465–484.

Bradshaw, J.Y., Kimbrough, D.L., 1989. Enriched: age constraints on metamorphism and the development of a metamorphic core complex in Fiordland, southern New Zealand; discussion. Geology 17, 380–381.

Bradshaw, J.Y., Kimbrough, D.L., 1991. Mid-Paleozoic age of granitoids in enclaves within Early Cretaceous granulites, Fiordland, southwest New Zealand. New Zealand Journal of Geology and Geophysics 34, 455–469.

Brown, E.H., 1996. High-pressure metamorphism caused by magma loading in Fiordland. New Zealand. Journal of Metamorphic Geology 14, 441–452.

Burchfield, B.C., Chen, Z., Hodges, K.V., Liu, Y., Royden, L.H., Deng, C., Xu, J., 1992. The South Tibetan detachment system, Himalayan orogen: extension contemporaneous with and parallel to shortening in a collisional mountain belt. Geological Society of America Special Paper 269, 1–41.

Burg, J.-P., Ford, M., 1997. Orogeny through time: an overview. In: Burg, J,-P., Ford, M. (Eds.), Orogeny Through Time. Geological Society of London, Special Publications 121, pp. 1–17.

Burg, J.-P., Brunel, M., Gapais, D., Chen, G.M., Li, G.H., 1984. Deformation of leucogranites of the crystalline Main Central Sheet in southern Tibet (China). Journal of Structural Geology 6, 535–542.

Clarke, G.L., Klepeis, K.A., Daczko, N.R., 2000. Cretaceous high-P granulites at Milford Sound, New Zealand: metamorphic history and emplacement in a convergent margin setting. Journal of Metamorphic Geology 18, 359–374.

Claypool, A., Klepeis, K.A., Dockrill, B., Clarke, G.L., Zwingmann, H., Tulloch, A., 2002. Structure and kinematics of oblique continental convergence in Northern Fiordland, New Zealand. Tectonophysics 359, 329–358.

Cooper, A.F., Barreiro, B.A., Kimbrough, D.L., Mattinson, J.M., 1987. Lamprophyre dike intrusion and the age of the Alpine fault, New Zealand. Geology 15, 941–944.

Cooper, R.A., 1979. Lower Paleozoic Rocks of New Zealand. Journal of the Royal Society of New Zealand 9, 29–84.

Cooper, R.A., Tulloch, A.J., 1992. Early Paleozoic terranes in New Zealand and their relationship to the Lachlan Fold Belt. Tectonophysics 214, 129–144.

Daczko, N.R., Klepeis, K.A., Clarke, G.L., 2001a. Evidence of Early Cretaceous collisional-style orogenesis in northern Fiordland, New Zealand and its effects on the evolution of the lower crust. Journal of Structural Geology 23, 693–713.

Daczko, N.R., Clarke, G.L., Klepeis, K.A., 2001b. Transformation of two-pyroxene hornblende granulite to garnet granulite involving simultaneous melting and fracturing of the lower crust, Fiordland, New Zealand. Journal of Metamorphic Geology 19, 547–560.

Daczko, N.R., Klepeis, K.A., Clarke, G.L., 2002a. Thermomechanical evolution of the crust during convergence and deep crustal pluton emplacement in the Western Province of Fiordland, New Zealand. Tectonics 21, 1–18.

Daczko, N.R., Stevenson, J.A., Clarke, G.L., Klepeis, K.A., 2002b. Successive hydration and dehydration of high-P mafic granofels involving clinopyroxene–kyanite symplectites, Mt. Daniel, Fiordland, New Zealand. Journal of Metamorphic Geology 20, 669–682.

Daczko, N.R., Klepeis, K.A., Clarke, G.L., 2002c. Kyanite–paragonite-bearing assemblages, northern Fiordland, New Zealand: rapid cooling at the lower crustal root of a Cretaceous magmatic arc. Journal of Metamorphic Geology 20, 887–902.

Davidson, C., Schmid, S.M., Hollister, L.S., 1994. Role of melt during deformation in the deep crust. Terra Nova 6, 133–142.

Dell'Angelo, L.N., Tullis, J., 1988. Experimental deformation of partially melted granitic aggregates. Journal of Metamorphic Geology 6, 495–516.

Ellis, S., Beaumont, C., Jamieson, R.A., Quinlan, G., 1998. Continental collision including a weak zone: the vise model and its application to the Newfoundland Appalachians. Canadian Journal of Earth Sciences 35, 1323–1346.

England, P., Houseman, G.A., 1989. Extension during continental convergence, with application to the Tibetan Plateau. Journal of Geophysical Research 94, 561–571.

Gibson, G.M., 1990. Uplift and exhumation of middle and lower crustal rocks in an extensional tectonic setting, Fiordland, New Zealand. In: Salisbury, M.H., Fountain, D.M. (Eds.), Exposed Cross-Sections of the Continental Crust. NATO ASI Series 317, Dordrecht, pp. 71–101.

Gibson, G.M., Ireland, T.R., 1995. Granulite formation during continental extension in Fiordland. Nature 375, 479–482.

Gibson, G.M., McDougall, I., Ireland, T.R., 1988. Age constraints on metamorphism and the development of a metamorphic core complex in Fiordland, southern New Zealand. Geology 16, 405–408.

Grindley, G.W., 1980. Geological map of New Zealand. Department of Scientific and Industrial Research Sheet, Wellington, New Zealand S13-Cobb, scale 1:63360.

Harrison, T.M., McDougall, I., 1980. Investigations of an intrusive contact, northwest Nelson, New Zealand. Thermal, chronological and isotopic constraints. Geochemica et Cosmochemica Acta 44, 1985–2003.

Harry, D.L., Oldow, J.S., Sawyer, D.S., 1995. The growth of orogenic belts and the role of crustal heterogeneities in decollement tectonics. Geological Society of America Bulletin 107, 1411–1426.

Hill, E.J., 1995. A deep crustal shear zone exposed in western Fiordland, New Zealand. Tectonics 14, 1172–1181.

Hollis, J.A., Clarke, G.L., Klepeis, K.A., Daczko, N.R., Ireland, T.R., 2003.

Geochronology and geochemistry of high-pressure granulites of the Arthur River Complex, Fiordland, New Zealand: Cretaceous magmatism and metamorphism on the Palaeo–Pacific margin. Journal of Metamorphic Geology 21, 299–313.

Hollis, J.A., Clarke, G.L., Klepeis, K.A., Daczko, N.R., Ireland, T.R., 2004. U–Pb zircon geochronology of Cretaceous granulites from Fiordland, New Zealand: rapid burial and uplift along the Mesozoic Pacific Gondwana margin. Journal of Metamorphic Geology, in press.

Huerta, A.D., Royden, L.H., Hodges, K.V., 1996. The interdependence of deformational and thermal processes in mountain belts. Science 273, 637–639.

Ireland, T.R., Gibson, G.M., 1998. SHRIMP monazite and zircon geochronology of high-grade metamorphism in New Zealand. Journal of Metamorphic Geology 16, 149–167.

Jamieson, R.A., Beaumont, C., Ellis, S., 1998. Partial melting in convergent orogens; thermal constraints and mechanical consequences. Geological Society of America Annual Meeting 30, 297.

Jiang, D., Williams, P.F., 1998. High-strain zones: a unified model. Journal of Structural Geology 20, 1105–1120.

Karlstrom, K.E., Williams, M.L., 1995. The case of simultaneous deformation, metamorphism and plutonism: an example from Proterozoic rocks in central Arizona. Journal of Structural Geology 17, 59–81.

Karlstrom, K.E., Williams, M.L., 2002. Nature of the middle crust-heterogeneity of structure and process due to pluton-enhanced tectonism: an example from Proterozoic rocks of the North American Southwest. In: Brown, M., Rushmer, T. (Eds.), Evolution and Differentiation of the Continental Crust. Cambridge University Press, in press.

Kimbrough, D.L., Tulloch, A.J., Coombs, D.S., Landis, C.A., Johnston, M.R., Mattinson, J.M., 1994. Uranium-lead zircon ages from the Median Tectonic Zone, New Zealand. New Zealand Journal of Geology andGeophysics 37, 393–419.

Klepeis, K.A., Crawford, M.L., 1999. High temperature, arc, parallel normal faulting at the roots of an obliquely convergent orogen. Geology 27, 7–10.

Klepeis, K.A., Daczko, N.R., Clarke, G.L., 1999. Kinematic vorticity and tectonic significance of superposed mylonites in a major lower crustal shear zone, northern Fiordland, New Zealand. Journal of Structural Geology 21, 1385–1405.

Klepeis, K.A., Clarke, G.L., Rushmer, T., 2003. Magma transport and coupling between deformation and magmatism in the continental lithosphere. GSA Today 13, 4–11.

Lamarche, G., Collot, J.-Y., Wood, R.A., Sossom, M., Sutherland, R., Delteil, J., 1997. The Oligocene–Miocene Pacific–Australia plate boundary, south of New Zealand: evolution from oceanic spreading to strike-slip faulting. Earth and Planetary Science Letters 148, 129–139.

Landis, C., Coombs, D.S., 1967. Metamorphic belts and orogenesis in southern New Zealand. Tectonophysics 4, 501–518.

Landis, C.A., Campbell, H.J., Aslund, T., Caywood, P.A., Douglas, A., Kimbrough, D.L., Pillai, D.D.L., Raine, J.I., Willsman, A., 1999. Permian–Jurassic strata at Productus Creek, Southland, New Zealand: implications for terrane dynamics of the eastern Gondwanaland margin. New Zealand Journal of Geology and Geophysics 42, 255–278.

Lin, S., Jiang, D., Williams, P.F., 1998. Transpression (or transtension) zones of triclinic symmetry: natural example and theoretical modelling. In: Holdsworth, R.E., Strachan, R.A., Dewey, J.F. (Eds.), Continental Transpressional and Transtensional Tectonics. Geological Society of London, Special Publications 135, pp. 41–47.

Ludwig, K.J., 2001. Isoplot/Ex (rev. 2.49). Berkeley Geochronology Center Special Publication No. 1a, 56pp.

Mattinson, J.L., Kimbrough, D.L., Bradshaw, J.Y., 1986. Western Fiordland orthogneiss: Early Cretaceous arc magmatism and granulite facies metamorphism, New Zealand. Contributions to Mineralogy and Petrology 92, 383–392.

Mayer, G., Mai, P.M., Plenefisch, T., Echtler, H., Luschen, E., Wehrle, V., Muller, B., Bonjer, K.P., Prodehl, C., Fuchs, K., 1997. The deep crust of the southern Rhine Graben: reflectivity and seismicity as images of dynamic processes. Tectonophysics 275, 15–40.

McCulloch, M.T., Bradshaw, J.Y., Taylor, S.R., 1987. Sm–Nd and Rb–Sr isotopic and geochemical systematics in Phanerozoic granulites from Fiordland, Southwest New Zealand. Contributions to Mineralogy and Petrology 97, 183–195.

McKenzie, D., Nimmo, F., Jackson, J.A., 2000. Characteristics and consequences of flow in the lower crust. Journal of Geophysical Research 105, 11,029–11,046.

Miller, R.B., Paterson, S.R., 2001. Influence of lithological heterogeneity, mechanical anisotropy, and magmatism on the rheology of an arc, North Cascades, Washington. Tectonophysics 342, 351–370.

Molnar, P., England, P., Martinod, J., 1993. Mantle dynamics, uplift of the Tibetan Plateau, and the Indian Monsoon. Reviews of Geophysics 31, 357–396.

Molnar, P., Anderson, H.J., Audoine, E., Eberhart-Phillips, D., Gledhill, K.R., Klosko, E.R., Mcevilly, T.V., Okaya, D., Savage, M.K., Stern, T., Wu, F.T., 1999. Continuous deformation versus faulting through the continental lithosphere of New Zealand. Science 286, 516–519.

Mortimer, N., Tulloch, A., 1996. The Mesozoic basement of New Zealand. Geological Society of Australia Extended Abstracts 43, 391–399.

Mortimer, N., Tulloch, A.J., Spark, R., Walker, N., Ladley, E., Kimbrough, D.L., Allibone, A.H., 1999a. Overview of the Median Batholith, New Zealand: a new interpretation of the geology of the Median Tectonic Zone and adjacent rocks. Journal of African Earth Sciences 29, 257–268.

Mortimer, N., Gans, P.B., Calvert, A., Walker, N., 1999b. Geology and thermochronometry of the east edge of the Median Batholith (Median Tectonic Zone); a new perspective on Permian to Cretaceous crustal growth of New Zealand. The Island Arc 8, 404–425.

Muir, R.J., Ireland, T.R., Weaver, S.D., Bradshaw, J.D., 1994. Ion microprobe U–Pb zircon geochronology of granitic magmatism in the Western Province of the South Island, New Zealand. Chemical Geology 113, 171–189.

Muir, R.J., Weaver, S.D., Bradshaw, J.D., Eby, G.N., Evans, J.A., 1995. The Cretaceous Separation Point Batholith, New Zealand; granitoid magmas formed by melting of mafic lithosphere. Journal of the Geological Society of London 152, 689–701.

Muir, R.J., Weaver, S.D., Bradshaw, J.D., Eby, G.N., Evans, J.A., Ireland, T.R., 1996. Geochemistry of the Karamea Batholith, New Zealand, and comparisons with the Lachlan Fold Belt granites of SE Australia. Lithos 39, 1–20.

Muir, R.J., Ireland, T.R., Weaver, S.D., Bradshaw, S.D., Evans, J.A., Eby, G.N., Shelley, D., 1998. Geochronology and geochemistry of a Mesozoic magmatic arc system, Fiordland, New Zealand. Journal of the Geological Society of London 155, 1037–1053.

Nathan, S., Thurlow, C., Warnes, P., Zucchetto, R., 2000. Geochronology database for New Zealand rocks (2nd edition): 1961–1999. Institute of Geological and Nuclear Sciences Report 11, p. 51.

Nemes, R., Neubauer, F., Cloetingh, S., Genser, J., 1997. The Klagenfurt Basin in the Eastern Alps: an intra-orogenic decoupled flexural basin? Tectonophysics 282, 189–203.

Norris, R.J., Cooper, A.F., 2001. Late Quaternary slip rates and slip partitioning on the Alpine Fault, New Zealand. Journal of Structural Geology 23, 507–520.

Oldow, J.S., Bally, A.W., Avé Lallemant, H.G., 1990. Transpression, orogenic float and lithospheric balance. Geology 18, 991–994.

Oliver, G.J.H., 1977. Feldspathic hornblende and garnet granulites and associated anorthosite pegmatites from Doubtful Sound, Fiordland, New Zealand. Contributions to Mineralogy and Petrology 65, 111–121.

Oliver, G.J.H., 1980. Geology of the granulite and amphibolite facies gneisses of Doubtful Sound, Fiordland, New Zealand. New Zealand Journal Geology and Geophysics 1, 27–41.

Oliver, G.J.H., 1990. An exposed cross-section of continental crust, Doubtful Sound, Fiordland, New Zealand; geophysical and geological setting. In: Salisbury, M.H., Fountain, D.M. (Eds.), Exposed Cross-

sections of the Continental Crust. NATO ASI Series 317, Dordrecht, pp. 43–69.

Oliver, G.J.H., Coggon, J.H., 1979. Crustal structure of Fiordland, New Zealand. Tectonophysics 54, 253–292.

Petford, N., Gallagher, K., 2001. Partial melting of mafic (amphibolitic) lower crust by periodic influx of basaltic magma. Earth and Planeteary Science Letters 193, 483–499.

Roering, C., van Reenen, D.D., Smit, C.A., Du Toit, R., 1995. Deep crustal embrittlement and fluid flow during granulite metamorphism in the Limpopo Belt, South Africa. Journal of Geology 103, 673–686.

Royden, L., 1996. Coupling and decoupling of crust and mantle in convergent orogens: implications for strain partitioning in the crust. Journal of Geophysical Research 101, 17,679–17,705.

Rushmer, T., 1995. An experimental deformation study of partially molten amphibolite: Applications to low-melt fraction segregation. In: Brown, M., Rushmer, T., Saywer, E.W. (Eds.), Mechanisms and Consequences of Melt Segregation from Crustal Protoliths. Journal of Geophysical Research 100, pp. 15,681–15,696.

Rutter, E.H., 1997. The influence of deformation on the extraction of crustal melts: a consideration of the role of melt-assisted granular flow. In: Holness, M. (Ed.), Deformation-enhanced Melt Segregation and Metamorphic Fluid Transport. The Mineralogical Society Series 8, pp. 82–110.

Rutter, E.H., Neumann, D.H.K., 1995. Experimental deformation of partially molten Westerly granite under fluid-absent conditions, with implications for the extraction of granitic magmas. In: Brown, M., Rushmer, T., Saywer, E.W. (Eds.), Mechanisms and Consequences of Melt Segregation from Crustal Protoliths. Journal of Geophysical Research 100, pp. 15,697–15,715.

Sisson, V.B., Pavlis, T.L., 1993. Geologic consequences of plate reorganization; an example from the Eocene Southern Alaska fore arc. Geology 21, 913–916.

Spear, S., 1993. Metamorphic Phase Equilibria and Pressure–Temperature–Time Paths. Mineralogical Society of America Monograph. pp. 1–799.

Spell, T.L., McDougall, I., Tulloch, A.J., 2000. Thermochronologic constraints on the breakup of the Pacific Gondwana margin: the Paparoa metamorphic core complex, South Island, New Zealand. Tectonics 19, 433–451.

Stacey, J.S., Kramers, J.D., 1975. Approximation of terrestrial lead isotope evolution by a two-stage model. Earth and Planetary Science Letters 26, 207–221.

Sutherland, R., 1995. The Australia–Pacific boundary and Cenozoic plate motions in the SW Pacific: some constraints from Geosat data. Tectonics 14, 819–831.

Sutherland, R., Davey, F., Beavan, J., 2000. Plate boundary deformation in South Island, New Zealand is related to inherited lithospheric structure. Earth and Planetary Science Letters 177, 141–151.

Teyssier, C., Tikoff, B., Weber, J., 2002. Attachment between brittle and ductile crust at wrenching plate boundaries. European Geophysical Society Special Publication 1, 119–144.

Tulloch, A.J., 1979. Plutonic and metamorphic rocks of the Victoria Range segment of the Karamea Batholith, southwest Nelson, New Zealand. Ph.D. thesis, University of Otago, New Zealand.

Tulloch, A.J., Challis, G.A., 2000. Emplacement depths of Paleozoic–Mesozoic plutons from western New Zealand estimated by hornblende-Al geobarometry. New Zealand Journal of Geology and Geophysics 43, 555–567.

Tulloch, A.J., Kimbrough, D.L., 1989. The Paparoa metamorphic core complex, New Zealand: Cretaceous extension associated with fragmentation of the Pacific margin of Gondwana. Tectonics 8, 1217–1234.

Tulloch, A.J., Kimbrough, D.L., 2003. Paired plutonic belts in convergent margins and the development of high Sr/Y magmatism: the Peninsular Ranges Batholith of California and the Median Batholith of New Zealand. Geological Society of America Special Paper, in press.

Tulloch, A.J., Ireland, T.R., Walker, N.W., Kimbrough, D.L., 2000. U–Pb zircon ages from the Milford Orthogneiss, Milford Sound, northern Fiordland: Paleozoic igneous emplacement and Early Cretaceous metamorphism. Institute of Geological and Nuclear Sciences Report 6, pp. 1–17.

Turnbull, I.M., 2000. Geology of the Wakatipu area. Institute of Geological and Nuclear Sciences geologic map 18, 1 sheet + pp. 72, Lower Hutt, New Zealand, scale 1:250,000.

Vanderhaeghe, O., Teyssier, C., 1997. Formation of the Shuswap metamorphic complex during late-orogenic collapse of the Canadian Cordillera: Role of ductile thinning and partial melting of the mid- to lower crust. Geodynamica Acta 10, 41–58.

Vanderhaeghe, O., Teyssier, C., 2001. Crustal-scale rheological transitions during late orogenic collapse. Tectonophysics 335, 211–228.

Waight, T.E., Weaver, S.D., Muir, R.J., 1998. Mid-Cretaceous granitic magmatism during the transition from subduction to extension in southern New Zealand: a chemical and tectonic synthesis. Lithos 45, 469–482.

Warner, M., 1990. Basalts, water, or shear zones in the lower continental crust? Tectonophysics 173, 163–174.

Wellman, H.W., 1953. Data for the study of recent and late Pleistocene faulting in the South Island of New Zealand. New Zealand Journal of Science and Technology B34, 270–288.

White, J.C., Jiang, D., 1994. High-strength ductile behavior of ancient lower continental crust: evidence from natural deformation. EOS Transactions of the American Geophysical Union 75, 329.

Wilks, K.R., Carter, N.L., 1990. Rheology of some continental lower crustal rocks. Tectonophysics 182, 57–77.

Willett, S.D., 1998. Geodynamic modeling and insight into deep crustal processes. Geological Society of America Annual Meeting 30, 243.

Williams, J.G., 1978. Eglinton Volcanics—stratigraphy, petrography and metamorphism. New Zealand Journal of Geology and Geophysics 21, 713–732.

Williams, J.G., Harper, C.T., 1978. Age and status of the Mackay Intrusives in the Eglinton–Upper Hollyford area. New Zealand Journal of Geology and Geophysics 21, 733–742.

Wood, B.L., 1972. Metamorphosed ultramafites and associated formations near Milford Sound, New Zealand. New Zealand Journal of Geology and Geophysics 15, 88–128.